Comparisons of several upwind schemes for multi-component one-dimensional inviscid flows

Didier Chargy, Remi Abgrall, Loula Fatima Fezoui, Bernard Larrouturou

INRIA

UNITÉ DE RECHERCHE
INRIA-SOPHIA ANTIPOLIS

Institut National
de Recherche
en Informatique
et en Automatique

Domaine de Voluceau
Rocquencourt
B.P. 105
78153 Le Chesnay Cedex
France
Tél.: (1) 39 63 55 11

Rapports de Recherche

Call Dif

N° 1253

Programme 7
Calcul Scientifique,
Logiciels Numériques et Ingénierie Assistée

COMPARISONS OF SEVERAL UPWIND SCHEMES FOR MULTI-COMPONENT ONE-DIMENSIONAL INVISCID FLOWS

Didier CHARGY
Rémi ABGRALL
Loula FEZOUI
Bernard LARROUTUROU

Juin 1990

RR-1253

COMPARISONS OF SEVERAL UPWIND SCHEMES FOR MULTI-COMPONENT ONE-DIMENSIONAL INVISID FLOWS

D. CHARGY[1], R. ABGRALL[2], L. FEZOUI[2] and B. LARROUTUROU[1]

(1) CERMICS, INRIA, SOPHIA-ANTIPOLIS, 06560 VALBONNE, FRANCE
(2) INRIA, SOPHIA-ANTIPOLIS, 06560 VALBONNE, FRANCE

COMPARISONS OF SEVERAL UPWIND SCHEMES FOR MULTI-COMPONENT ONE-DIMENSIONAL INVISCID FLOWS

Didier CHARGY, Rémi ABGRALL, Loula FEZOUI, Bernard LARROUTUROU

ABSTRACT: We present detailed comparisons of three classes of numerical schemes for the computation of mixture flows. The differences between these schemes mainly concern the discrete coupling between the Euler equations (written for the mixture) and the additional conservation equations which describe the convection of the gaseous species. The best results are given by the class of schemes which preserve the maximum principle for the mass fractions of all species.

COMPARAISONS DE METHODES NUMERIQUES DECENTREES POUR LE CALCUL D'ECOULEMENTS DE MELANGES GAZEUX

Didier CHARGY, Rémi ABGRALL, Loula FEZOUI, Bernard LARROUTUROU

RESUME: Nous présentons des comparaisons détaillées entre trois classes de méthodes numériques décentrées pour le calcul d'écoulements de mélanges gazeux. Les différences entre ces trois familles de méthodes concernent surtout le couplage discret entre les équations d'Euler (écrites pour le mélange) et les équations de conservation supplémentaires qui décrivent la convection des espèces gazeuses. Les meilleurs résultats sont obtenus en utilisant la classe des schémas numériques qui préservent le principe du maximum pour les fractions massiques de toutes les espèces.

Contents

1 INTRODUCTION

We consider in this report the numerical approximation of the following system of the "multi-component Euler equations":

$$\begin{cases} \rho_t + (\rho u)_x = 0 \,, \\ (\rho u)_t + (\rho u^2 + p)_x = 0 \,, \\ E_t + [u(E+p)]_x = 0 \,, \\ (\rho Y)_t + (\rho u Y)_x = 0 \,, \end{cases} \tag{1}$$

which describes the one-dimensional inviscid flow of a mixture of two gaseous species (see the definition of the notations below). This study is a stepping stone towards more complex investigations of mixture flows where the hyperbolic aspects play a major role, such as transonic reactive flows (see e.g. [5]), hypersonic flows (see e.g. [2], [4], [7], [11], [19]) or detonations (see e.g. [18]).

After having presented some basic facts about system (1) and the associated Riemann problem in Section 2, we will describe in detail in Section 3 three different classes of numerical methods for the solution of (1); all presented schemes rely on the existing upwind schemes which have been developed for the single-component Euler equations: we will consider the schemes of Osher [20], Roe [21] and Van Leer [27]. The second-order accurate extension of these schemes is described in Section 4, while Section 5 is devoted to detailed numerical comparisons, for two different multi-component shock tube problems.

2 THE MULTI-COMPONENT EULER EQUATIONS

We consider in this section the one-dimensional inviscid flow of a mixture of N species Σ_1, Σ_2, ... Σ_N. We will always assume in the sequel that all species in the mixture are at thermal equilibrium (in other words, that we can use a single temperature, which may vary in space and time, but which is the same for all species), that the total pressure in the mixture is the sum of the partial pressures of the individual components (Dalton's law), and that each component behaves as a perfect gas. Moreover, we temporarily neglect the effects of diffusion and chemical reactions in the gaseous mixture.

2.1 Governing equations

The governing equations for this flow express the conservation of mass for each component, the conservation of momentum and of the total energy. They take the form (see e.g. [29]):

$$\begin{cases} (\rho Y_k)_t + (\rho u Y_k)_x = 0 \quad \text{for } 1 \le k \le N \,, \\ (\rho u)_t + (\rho u^2 + p)_x = 0 \,, \\ \mathcal{E}_t + [u(\mathcal{E}+p)]_x = 0 \,, \end{cases} \tag{2}$$

where ρ is the mixture density, Y_k is the mass fraction of species Σ_k (that is, ρY_k is the separate density of species Σ_k, and $\sum_{k=1}^{N} Y_k = 1$), u is the mixture velocity (which is also the velocity of each species, since we neglect molecular diffusion), p is the total pressure in the mixture, and $\mathcal{E}$ is the total energy per unit volume.

As already said, we assume here that each species Σ_k obeys the perfect gas laws, and in particular has constant specific heats at constant volume and pressure C_{vk} and C_{pk}. We will also denote γ_k the ratio $\gamma_k = \dfrac{C_{pk}}{C_{vk}}$, and M_k the molecular weight of species Σ_k, which satisfies Mayer's relation:

$$M_k(C_{pk} - C_{vk}) = R \; ; \tag{3}$$

R is the universal gas constant. The total pressure p is then given by Dalton's law:

$$p = \sum_{k=1}^{N} p_k \; , \tag{4}$$

the partial pressure p_k of species Σ_k being given by:

$$p_k = \rho Y_k \frac{R}{M_k} T \; ; \tag{5}$$

T is the temperature of the mixture. Considering that the N species may have different specific heats of formation h_k^0 , we write the total energy $\mathcal{E}$ as (see e.g. [29]):

$$\mathcal{E} = \sum_{k=1}^{N} \left(\frac{1}{2} \rho Y_k u^2 + \rho Y_k C_{vk} T + \rho Y_k h_k^0 \right) \; . \tag{6}$$

Since the temperature and the partial pressures do not appear in the conservation relations (2), we can eliminate them and consider that, in equations (2), the pressure p is given by the following relation, which is deduced from (3)-(6):

$$p = (\gamma - 1) \left(\mathcal{E} - \frac{1}{2} \rho u^2 - \sum_{k=1}^{N} \rho Y_k h_k^0 \right) \; , \tag{7}$$

γ being the local ratio of the specific heats of the mixture:

$$\gamma = \frac{(C_p)_{mixture}}{(C_v)_{mixture}} = \frac{\sum\limits_k Y_k C_{pk}}{\sum\limits_k Y_k C_{vk}} = \frac{\sum\limits_k Y_k C_{vk} \gamma_k}{\sum\limits_k Y_k C_{vk}} \; . \tag{8}$$

The last equality in (8) shows that the local value of γ (which depends on the mixture composition) is a linear convex combination of the γ_k's.

System (2)-(7) (with γ given by (8)) can be rewritten in a different way. Defining E as the sum of the kinetic and thermal energies per unit volume:

$$E = \frac{1}{2}\rho u^2 + \sum_{k=1}^{N} \rho Y_k \, C_{vk} T = \mathcal{E} - \sum_{k=1}^{N} \rho Y_k h_k^0 \, , \tag{9}$$

we can rewrite (2)-(7) as:

$$\begin{cases} (\rho Y_k)_t + (\rho u Y_k)_x = 0 \quad \text{for} \;\; 1 \leq k \leq N \, , \\ (\rho u)_t + (\rho u^2 + p)_x = 0 \, , \\ E_t + [u(E+p)]_x = 0 \, , \end{cases} \tag{10}$$

$$p = (\gamma - 1)\left(E - \frac{1}{2}\rho u^2\right) \, , \tag{11}$$

(the energy equation in (10) is a linear combination of the energy and species conservation equations in (2)). Summing all species equations in (10), one can also get an equation for the total density ρ and rewrite (10) as:

$$\begin{cases} \rho_t + (\rho u)_x = 0 \, , \\ (\rho u)_t + (\rho u^2 + p)_x = 0 \, , \\ E_t + [u(E+p)]_x = 0 \, , \\ (\rho Y_k)_t + (\rho u Y_k)_x = 0 \quad \text{for} \;\; 1 \leq k \leq N-1 \, . \end{cases} \tag{12}$$

Remark 1: At this point, one may wonder if the three systems of conservation laws (2), (10) and (12) are really equivalent, from both points of view of the exact solutions of the corresponding initial value problem and of their numerical approximation using conservative schemes. The answer is of course positive, since only *linear* combinations of the *conservative* equations are used to transform one of these systems into another. Indeed, if we denote $W_t + F_x = 0$, with $W \in I\!R^{N+2}$, $F \in I\!R^{N+2}$ the vector form of (2), system (10) can be written in the form $\mathcal{W}_t + \mathcal{F}_x = 0$, with $\mathcal{W} = MW$ and $\mathcal{F} = MF$, M being an $N+2 \times N+2$ non singular matrix *which is independent of* W. It is then straightforward to check that solving an initial value problem for $W_t + F_x = 0$, either exactly or using any of the first-order accurate conservative schemes considered below, is equivalent to solving it for the transformed system $\mathcal{W}_t + \mathcal{F}_x = 0$ (this conclusion is no more true with the limited second-order accurate schemes discussed in Section 4; see Sections 5 below).

This shows that using instead of (10) the system (12), where the N^{th} species does not play the same role as the other $N-1$ components, has no importance, from both mathematical and numerical points of view. The preceding arguments also show that treating the system (2)-(7) where the N species have different heats of formation exactly amounts to treating the system (10)-(11) where all heats of formation are equal to 0. •

We will in fact use the form (12) where the three first equations are the classical Euler equations, written here for the mixture.

2.2 Homogeneity and hyperbolicity

From now on, we will restrict our attention to the case of a mixture made of only two species Σ_1 and Σ_2. But all results presented below can be straightforwardly extended to mixtures consisting of any number of components N. Simply denoting Y the mass fraction Y_1 of the first species, we obtain the system (13):

$$\begin{pmatrix} \rho \\ \rho u \\ E \\ \rho Y \end{pmatrix}_t + \begin{pmatrix} \rho u \\ \rho u^2 + p \\ u(E+p) \\ \rho u Y \end{pmatrix}_x = 0 \,, \tag{13}$$

with:

$$p = (\gamma - 1)\left(E - \frac{1}{2}\rho u^2\right) \,, \tag{14}$$

and:

$$\gamma = \frac{Y C_{v1}\gamma_1 + (1-Y)C_{v2}\gamma_2}{Y C_{v1} + (1-Y)C_{v2}} \,. \tag{15}$$

We will use the classical notations W and F for the vectors of the conservative variables and of the fluxes:

$$W = \begin{pmatrix} \rho \\ \rho u \\ E \\ \rho Y \end{pmatrix} = \begin{pmatrix} W^1 \\ W^2 \\ W^3 \\ W^4 \end{pmatrix} = , \quad F = \begin{pmatrix} \rho u \\ \rho u^2 + p \\ u(E+p) \\ \rho u Y \end{pmatrix} = \begin{pmatrix} F^1 \\ F^2 \\ F^3 \\ F^4 \end{pmatrix} \,. \tag{16}$$

Then, we have the two following simple results, which are shown in e.g. [1], [3], [4], [9], [17]:

Proposition 1:

The flux vector F is an homogeneous function of degree 1 of W. •

Proposition 2:

If the specific heat ratio γ_k of each species in the mixture satisfies the inequality:

$$\gamma_k > 1 \,, \tag{17}$$

then the system (1.1) is hyperbolic. •

The proof of these results is straightforward. We will simply mention here that one can write:

$$\gamma = \frac{W^4 C_{v1}\gamma_1 + (W^1 - W^4)C_{v2}\gamma_2}{W^4 C_{v1} + (W^1 - W^4)C_{v2}} = \gamma(W) \,, \tag{18}$$

that the function $\gamma(W)$ is homogeneous of degree 0, which implies that F is homogeneous of degree 1, as in the single component case:

$$\forall r > 0\ ,\quad F(rW) = rF(W)\ . \tag{19}$$

Then, the Jacobian matrix $A(W) = \dfrac{DF}{DW}$ has the following expression:

$$A(W) = \begin{pmatrix} 0 & 1 & 0 & 0 \\ \dfrac{(\gamma-3)}{2}u^2 + X & (3-\gamma)u & \gamma - 1 & X' \\ \dfrac{(\gamma-1)}{2}u^3 - uH + uX & H - (\gamma-1)u^2 & \gamma u & uX' \\ -uY & Y & 0 & u \end{pmatrix} \tag{20}$$

we have set $H = \dfrac{E+p}{\rho}$ (H is the specific enthalpy of the mixture), $X = \dfrac{p}{\gamma - 1}\dfrac{\partial \gamma}{\partial W^1}$, $X' = \dfrac{p}{\gamma - 1}\dfrac{\partial \gamma}{\partial W^4}$, where γ is given by (18). A straightforward calculation then shows that the eigenvalues of $A(W)$ are:

$$\lambda_1 = u - c\ ,\quad \lambda_2 = u\ ,\quad \lambda_3 = u\ ,\quad \lambda_4 = u + c\ , \tag{21}$$

where the sound speed c has the usual expression:

$$c = \sqrt{\frac{\gamma p}{\rho}}\ , \tag{22}$$

but with $\gamma = \gamma(W)$. We should say at this point that this expression of the sound speed in the two-component mixture, which we have derived by evaluating the eigenvalues of the flux Jacobian matrix A, is equivalent to the usual expression $c = \dfrac{\partial p}{\partial \rho}\,|_S$ (derivative at constant entropy; see e.g. [6]).

A set of right eigenvectors is easily found; one can take:

$$r_1 = \begin{pmatrix} 1 \\ u - c \\ H - uc \\ Y \end{pmatrix}\ ,\quad r_2 = \begin{pmatrix} 1 \\ u \\ \dfrac{u^2}{2} - \dfrac{X}{\gamma - 1} \\ 0 \end{pmatrix}\ ,\quad r_3 = \begin{pmatrix} 0 \\ 0 \\ -\dfrac{X'}{\gamma - 1} \\ 1 \end{pmatrix}\ ,\quad r_4 = \begin{pmatrix} 1 \\ u + c \\ H + uc \\ Y \end{pmatrix}\ , \tag{23}$$

(of course, any combination of r_2 and r_3 is also a right eigenvector associated to the eigenvalue u).

Remark 2: The following relations are easy to check and will be useful in the sequel:

$$H = \frac{u^2}{2} + \frac{c^2}{\gamma - 1}\,, \tag{24}$$

$$X' = \frac{p}{\gamma - 1}\,\frac{C_{v1}C_{v2}(\gamma_1 - \gamma_2)}{\rho[YC_{v1} + (1-Y)C_{v2}]^2} = \frac{C_{v1}C_{v2}(\gamma_1 - \gamma_2)T}{YC_{v1} + (1-Y)C_{v2}}\,. \quad \bullet \tag{25}$$

2.3 The multi-component Riemann problem

Let us now examine the solution of a Riemann problem for system (13). Using again the notations (16) and introducing two states W_L and W_R, we consider the problem:

$$\begin{cases} W_t + F(W)_x = 0 \quad \text{for } x \in I\!R\,, \quad t \geq 0\,, \\ W(x,0) = \begin{cases} W_L & \text{if } x < 0\,, \\ W_R & \text{if } x > 0\,. \end{cases} \end{cases} \tag{26}$$

This problem is solved in [1], [3], [17]. Its exact solution $W^{\mathcal{R}}(x,t)$ is presented on Figure 1. It is of course self-similar (i.e. $W^{\mathcal{R}}(x,t)$ only depends on the ratio $\frac{x}{t}$), and consists, as in the single-component case, of four constant states $W_{(1)}$, $W_{(2)}$, $W_{(3)}$, $W_{(4)}$ separated by shocks, rarefaction waves or a contact discontinuity. More precisely, as shown on Figure 1, $W_{(1)} = W_L$ and $W_{(2)}$ are separated by a 1-wave (i.e. a wave associated with the first characteristic field, either a 1-shock or a 1-rarefaction wave); $W_{(2)}$ and $W_{(3)}$ are separated by a 2-discontinuity or contact discontinuity; and $W_{(3)}$ and $W_{(4)} = W_R$ are separated by a 4-wave. Also, the pressure p and the velocity u are continuous across the contact discontinuity. Last but not least, the mass fraction Y remains constant across the 1-wave and the 4-wave (whatever these waves are, shocks or rarefactions), and only varies across the contact discontinuity.

3 FIRST-ORDER ACCURATE UPWIND NUMERICAL SCHEMES

Let us now consider the numerical solution of an initial value problem associated with system (13):

$$\begin{cases} W_t + F(W)_x = 0 \quad \text{for } x \in I\!R\,, \quad t \geq 0\,, \\ W(x,0) = W^0(x) \quad \text{for } x \in I\!R\,. \end{cases} \tag{27}$$

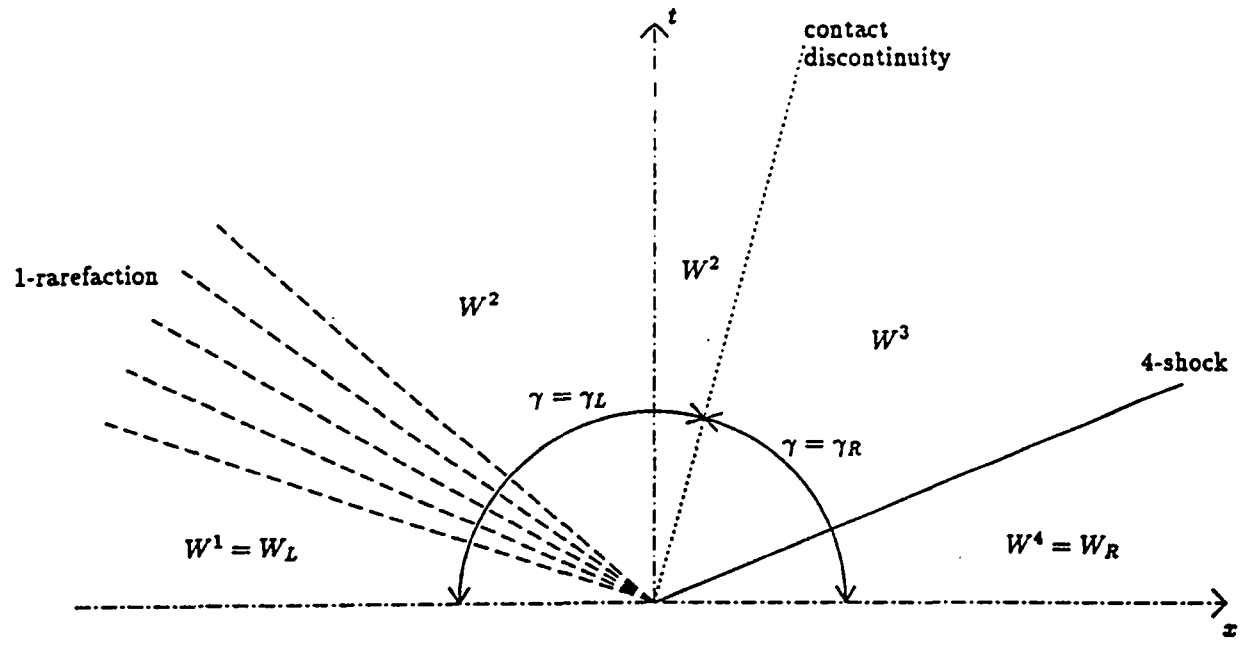

Figure 1: The solution $W^{\mathcal{R}}$ of the multi-component Riemann problem.

We will restrict our attention in this section to explicit, three-point, first-order accurate schemes written in conservative form. In other words, using very classical notations, we consider numerical schemes of the form:

$$\frac{W_j^{n+1} - W_j^n}{\Delta t} + \frac{\phi_{j+1/2} - \phi_{j-1/2}}{\Delta x} = 0 \,, \tag{28}$$

where the numerical flux $\phi_{j+1/2}$ is evaluated using a "numerical flux function" Φ:

$$\phi_{j+1/2} = \Phi(W_j^n, W_{j+1}^n) \,. \tag{29}$$

(we write $\phi_{j+1/2}$ instead of $\phi_{j+1/2}^n$ for simplicity).

There exists many schemes of this type for the single-component Euler equations (see for instance [13] and the references mentioned below). We are going to consider three of these schemes, namely the Van Leer, Roe and Osher schemes, and we will describe three different ways of extending each of them to the solution of the multi-component system (13).

3.1 The three basic Euler schemes

For the sake of completeness, we first briefly recall the definition of each of the considered schemes for the Euler equations, using the notations:

$$U = \begin{pmatrix} \rho \\ \rho u \\ E \end{pmatrix}, \quad G = \begin{pmatrix} \rho u \\ \rho u^2 + p \\ u(E+p) \end{pmatrix}. \tag{30}$$

We will set:

$$B(U) = \frac{DG}{DU} = \begin{pmatrix} 0 & 1 & 0 \\ \frac{(\gamma-3)}{2}u^2 & (3-\gamma)u & \gamma - 1 \\ \frac{(\gamma-1)}{2}u^3 - uH & H - (\gamma-1)u^2 & \gamma u \end{pmatrix}. \tag{31}$$

3.1.1 The Van Leer scheme

Van Leer [27] introduced a continuously differentiable flux-splitting scheme, defined by the flux function:

$$\Phi(U_L, U_R) = G_+(U_L) + G_-(U_R), \tag{32}$$

where G_+ and G_- satisfy $G(U) = G_+(U) + G_-(U)$ and are given by the following expressions:

* if $u \geq c$, $G_+(U) = G(U)$, $G_-(U) = 0$;

* if $-c \leq u \leq c$,

$$G_+(U) = \begin{pmatrix} G_+^1 \\ G_+^2 \\ G_+^3 \end{pmatrix} = \begin{pmatrix} \frac{\rho}{4c}(u+c)^2 \\ G_+^1\left(u - \frac{u-2c}{\gamma}\right) \\ \frac{\gamma^2}{2(\gamma^2-1)}\frac{(G_+^2)^2}{G_+^1} \end{pmatrix}, \tag{33}$$

$$G_-(U) = \begin{pmatrix} G_-^1 \\ G_-^2 \\ G_-^3 \end{pmatrix} = \begin{pmatrix} -\frac{\rho}{4c}(u-c)^2 \\ G_-^1\left(u - \frac{u+2c}{\gamma}\right) \\ \frac{\gamma^2}{2(\gamma^2-1)}\frac{(G_-^2)^2}{G_-^1} \end{pmatrix}; \tag{34}$$

* if $u \leq -c$, $G_+(U) = 0$, $G_-(U) = G(U)$.

3.1.2 The Roe scheme

Roe [21] has proposed a conservative upwind scheme which uses an approximate Riemann solver based on a linearization of the fluxes (see [21] and also [13]). The numerical flux function of this scheme has the form:

$$\Phi(U_L, U_R) = \frac{G(U_L) + G(U_R)}{2} + \frac{1}{2}|\tilde{B}|(U_L - U_R) , \tag{35}$$

where $\tilde{B} = \tilde{B}(U_L, U_R)$ is a diagonalisable matrix which satisfies the property:

$$G(U_L) - G(U_R) = \tilde{B}(U_L - U_R) . \tag{36}$$

We have used in (35) a classical notation: if C is a diagonalisable matrix, the matrix $|C|$ is defined as follows: the diagonalisation of C is written as $C = T\Lambda T^{-1}$, where Λ is the diagonal matrix $\Lambda = Diag[\mu_1, \mu_2 \cdots \mu_n]$, and one sets $|C| = T|\Lambda|T^{-1}$, where $|\Lambda| = Diag[|\mu_1|, |\mu_2| \cdots |\mu_n|]$.

There are several different ways of choosing a matrix $\tilde{B}$ satisfying (36). Roe [21] proposed to define $\tilde{B}$ as follows: $\tilde{B}$ is equal to the flux Jacobian matrix B evaluated for some state $\tilde{U} = \tilde{U}(U_L, U_R)$ known as "Roe's average of U_L and U_R". More precisely $\tilde{B} = B[\tilde{U}(U_L, U_R)]$, where $\tilde{U} = (\tilde{\rho}, \tilde{\rho}\tilde{u}, \tilde{E})^T$ is defined by the relations:

$$\tilde{\rho} = \frac{\rho_1\sqrt{\rho_1} + \rho_2\sqrt{\rho_2}}{\sqrt{\rho_1} + \sqrt{\rho_2}} , \quad \tilde{u} = \frac{u_1\sqrt{\rho_1} + u_2\sqrt{\rho_2}}{\sqrt{\rho_1} + \sqrt{\rho_2}} , \tag{37}$$

$$\tilde{H} = \frac{H_1\sqrt{\rho_1} + H_2\sqrt{\rho_2}}{\sqrt{\rho_1} + \sqrt{\rho_2}} , \tag{38}$$

(in fact, defining $\tilde{\rho}$ is not useful here since only $\tilde{u}$ and $\tilde{H}$ are needed to evaluate the Jacobian matrix $B(\tilde{U})$).

3.1.3 The Osher scheme

The scheme proposed by Osher and Solomon [20], which is referred to as the Osher scheme, is based on the following expression of the numerical flux function:

$$\Phi(U_L, U_R) = \frac{G(U_L) + G(U_R)}{2} - \frac{1}{2}\int_{U_L}^{U_R} |B(U)|dU , \tag{39}$$

where the integration is carried out on a path connecting U_L and U_R in the state-space. The integration path proposed in [20] is piecewise parallel to the right eigenvectors of the flux Jacobian matrix B, and the evaluation of the integral in (39) relies on the knowledge of the Riemann invariants associated with each eigenvectors (see [20] for more details). In fact, two different "Osher schemes" exist: in the original scheme of Osher-Solomon [20], the path connecting U_L and U_R is piecewise parallel to r_3 the right eigenvector corresponding to $u + c$, r_2 (corresponding to u) and r_1 (corresponding to $u - c$) in this order. On the opposite, one can also define a so-called "physical Osher" scheme by choosing a path which is piecewise parallel to r_1, r_2 and r_3 in this order (see e.g. [24] and Appendix A for more details).

3.2 A first multi-component extension: the uncoupled approach

A first and simple approach to the numerical solution of (13) has been used in e.g. [12]. It consists in treating separately at each time step the Euler equations and the species equation in (13). In the sequel, this approximation will be referred to as the "uncoupled approach" or "approach (A)".

For the Euler equations, one uses one of the classical single-component "Euler schemes" presented in the preceding section, with a "frozen γ". This means that, for the evaluation of the first three components of $\phi_{i+1/2}$ at time t^n, one uses the flux of one of the above Euler schemes computed using a frozen value $\gamma_{i+1/2} = \gamma\left(\frac{Y_i^n + Y_{i+1}^n}{2}\right)$.

Beside this, one uses an upwind approximation of the donor-cell type for the species equation; defining $u_{i+1/2}^n = \frac{1}{2}(u_i^n + u_{i+1}^n)$, one evaluates the fourth component $\phi_{i+1/2}^4$ of $\phi_{i+1/2}$ by:

$$\phi_{i+1/2}^4 = u_{i+1/2}^n \times \begin{cases} (\rho Y)_i^n & \text{if } u_{i+1/2}^n > 0, \\ (\rho Y)_{i+1}^n & \text{if } u_{i+1/2}^n < 0. \end{cases} \tag{40}$$

This donor-cell approximation is based on the non conservative form $Y_t + uY_x = 0$ of the species equation (which can be obtained using the first and fourth equation in (13)): the variable Y is purely convected by the flow.

Another possibility is to use instead of $u_{i+1/2}^n$ the Roe averaged velocity:

$$\tilde{u}_{i+1/2}^n = \frac{u_i^n \sqrt{\rho_i^n} + u_{i+1}^n \sqrt{\rho_{i+1}^n}}{\sqrt{\rho_i^n} + \sqrt{\rho_{i+1}^n}}, \tag{41}$$

and evaluate $\phi_{i+1/2}^4$ as:

$$\phi_{i+1/2}^4 = \tilde{u}_{i+1/2}^n \times \begin{cases} (\rho Y)_i^n & \text{if } \tilde{u}_{i+1/2}^n > 0, \\ (\rho Y)_{i+1}^n & \text{if } \tilde{u}_{i+1/2}^n < 0. \end{cases} \tag{42}$$

It is easy to see that approach (A) preserves the mass fraction positivity (if $Y_j^n \geq 0$ for all j, then $Y_j^{n+1} \geq 0$ for all j), under an appropriate CFL condition (see [15]).

3.3 A second multi-component extension: the fully coupled approach

In this second approach, we do not treat any longer the Euler equations and the species equation separately: instead, we consider the whole system (13) as an hyperbolic system of coupled non linear conservation laws and extend to this bigger system the three basic Euler

schemes described in Section 3.1. We will refer to this class of schemes as the "fully-coupled approach" or "approach (B)".

Remark 3: Of course, since we can compute the exact solution of the Riemann problem (26), we could also define a "fully-coupled Godunov scheme": calling $\mathcal{W}(\sigma; W_L, W_R))$ the value of $W^{\mathcal{R}}(\sigma t, t)$, which is independent of t for any $\sigma \in I\!R$ and $t > 0$, we would simply set $\Phi(W_L, W_R) = \mathcal{W}(0; W_L, W_R)$. •

3.3.1 The multi-component Van Leer scheme

A natural extension of the Van Leer flux decomposition to the multi-component case is proposed in [17]. One simply sets:

$$\Phi(W_L, W_R) = F_+(W_L) + F_-(W_R)\ , \tag{43}$$

where $F_+(W) = F(W)$ when $u \geq c$, $F_+(W) = 0$ when $u \leq -c$, and:

$$F_+(W) = \begin{pmatrix} F_+^1 \\ F_+^2 \\ F_+^3 \\ F_+^4 \end{pmatrix} = \begin{pmatrix} \dfrac{\rho}{4c}(u+c)^2 \\ F_+^1\left(u - \dfrac{u-2c}{\gamma}\right) \\ \dfrac{\gamma^2}{2(\gamma^2-1)}\dfrac{(F_+^2)^2}{F_+^1} \\ Y F_+^1 \end{pmatrix}, \tag{44}$$

when $-c \leq u \leq c$. In (44), γ is the *local* (non constant) specific heat ratio (18). The split flux F_- is defined by analogous formulae (or by the identity $F = F_+ + F_-$). As in the single-component case, we also have here the property that, if all characteristic wave speeds associated with the state W are positive (resp. negative), i.e. if $u \geq c$ (resp $u \leq -c$), then $F_+(W) = F(W)$ (resp. $F_-(W) = F(W)$). At this point also arises the question of the validity of this flux decomposition, or of the stability of the resulting scheme: the scheme uses an upward (resp. downward) differencing for F_+ (resp. F_-), because all wave speeds associated with F_+ (resp. F_-) are expected to be positive (resp. negative). But is it actually the case ? The answer is given by the next result, which extends to multi-component flows the result shown by Van Leer [26] in the single-component case (see [17] for the proof):

Proposition 3:

If the specific heat ratio γ_k of each species in the mixture satisfies the inequality $1 < \gamma_k < 3$, then all eigenvalues of the Jacobian matrix $\dfrac{DF^+}{DW}$ (resp. $\dfrac{DF^-}{DW}$) are real and positive (resp. negative). •

3.3.2 The multi-component Roe scheme

The extension of Roe's scheme to the two-component system (13) has been derived in [1] and [9]. The two-component scheme relies on the relations:

$$\Phi(W_L, W_R) = \frac{F(W_L) + F(W_R)}{2} + \frac{1}{2}|\tilde{A}|(W_L - W_R)\,, \tag{45}$$

where $\tilde{A} = \tilde{A}(W_L, W_R)$ satisfies the property:

$$F(W_L) - F(W_R) = \tilde{A}(W_L - W_R)\,. \tag{46}$$

Again we can define the averaged state $\tilde{W} = (\tilde{\rho}, \tilde{\rho}\tilde{u}, \tilde{E}, \tilde{\rho}\tilde{Y})^T$ by:

$$\tilde{\rho} = \frac{\rho_L\sqrt{\rho_L} + \rho_R\sqrt{\rho_R}}{\sqrt{\rho_L} + \sqrt{\rho_R}}\,, \quad \tilde{u} = \frac{u_L\sqrt{\rho_L} + u_R\sqrt{\rho_R}}{\sqrt{\rho_L} + \sqrt{\rho_R}}\,, \tag{47}$$

$$\tilde{H} = \frac{H_L\sqrt{\rho_L} + H_R\sqrt{\rho_R}}{\sqrt{\rho_L} + \sqrt{\rho_R}}\,, \tag{48}$$

$$\tilde{Y} = \frac{Y_L\sqrt{\rho_L} + Y_R\sqrt{\rho_R}}{\sqrt{\rho_L} + \sqrt{\rho_R}}\,, \tag{49}$$

(again determining $\tilde{\rho}$ is not necessary). But in this two-component context (unless both species in the mixture have the same specific heat ratio $\gamma_1 = \gamma_2$, that is unless $\gamma = \gamma(W)$ is a constant), the flux Jacobian matrix $A(\tilde{W})$ does not satisfy property (46). Therefore, the matrix $\tilde{A}$ is to be chosen different from $A(\tilde{W})$ (but close to the latter since we want our extension to reduce to the usual Roe scheme when both species are the same). The result, given in [1], [9] is the following:

$$\tilde{A} = \begin{pmatrix} 0 & 1 & 0 & 0 \\ \dfrac{(\tilde{\gamma}-3)}{2}\tilde{u}^2 - \tilde{Y}\tilde{X}' & (3-\tilde{\gamma})\tilde{u} & \tilde{\gamma}-1 & \tilde{X}' \\ -\tilde{u}\tilde{H} + \dfrac{(\tilde{\gamma}-1)}{2}\tilde{u}^3 - \tilde{u}\tilde{Y}\tilde{X}' & \tilde{H} - (\tilde{\gamma}-1)\tilde{u}^2 & \tilde{\gamma}\tilde{u} & \tilde{u}\tilde{X}' \\ -\tilde{u}\tilde{Y} & \tilde{Y} & 0 & \tilde{u} \end{pmatrix}, \tag{50}$$

where $\tilde{\gamma} = \gamma(\tilde{W})$, but where $\tilde{X}'$ is not equal to $X'(\tilde{W})$ given by (25). In order to insure that property (46) holds, one has to choose:

$$\tilde{X}' = \frac{C_{v1}C_{v2}(\gamma_1 - \gamma_2)\tilde{T}}{\tilde{Y}C_{v1} + (1-\tilde{Y})C_{v2}}\,, \tag{51}$$

(compare with (25)), with:

$$\tilde{T} = \frac{T_L\sqrt{\rho_L} + T_R\sqrt{\rho_R}}{\sqrt{\rho_L} + \sqrt{\rho_R}} \neq T(\tilde{W}) \ . \tag{52}$$

The matrix $\tilde{A}$ defined by (50)-(52) is then diagonalisable: its eigenvalues are $\tilde{u} - \tilde{c}$, $\tilde{u}$, $\tilde{u}$, $\tilde{u} + \tilde{c}$, where $\tilde{c}^2 = (\tilde{\gamma} - 1)\left(\tilde{H} - \frac{\tilde{u}^2}{2}\right)$ from (24) (it is easy to check that this quantity is positive), and its eigenvectors are given by expressions which are analogous to (23). We leave it to the reader to check that $\tilde{A}$ defined by (50)-(52) actually satisfies (46) (the details of the proof can also be found in [1]).

Remark 4: We have said in Remark 1 that both systems (10) (with one equation for each species) and (12) (with one equation for the mixture density ρ and one equation for all but one species) are equivalent. Of course we found it helpful for all preceding calculations to use system (12) whose first three equations have the form of the usual Euler equations. But this formulation (12) (or (13) in the case of two species) also has a small drawback: the expression (51) for the extended Roe scheme is less easy to extend to N-component mixtures that the expression given in [1] , which is equivalent to (51), but which is derived by using a system written under the form (10) where all species play the same role. •

3.3.3 The multi-component Osher scheme

The extension of the Osher scheme to multi-component flows has been done in [3]. The extended scheme is of course defined by the analogue of (39):

$$\Phi(W_L, W_R) = \frac{F(W_L) + F(W_R)}{2} - \frac{1}{2}\int_{W_L}^{W_R} |A(W)| dW \ , \tag{53}$$

and the evaluation of the integral again uses the Riemann invariants. Let us recall here that $\phi^{(m)} = \phi^{(m)}(W)$ is an m-Riemann invariant if:

$$\nabla_W \phi^{(m)}(W).r_m(W) = \sum_{l=1}^{4} \frac{\partial \phi^{(m)}}{\partial W_l}.(r_m)_l = 0 \ ; \tag{54}$$

as a consequence, a m-Riemann invariant is constant along a curve $W(s)$ in the state-space which is parallel to the m^{th} right eigenvector of the Jacobian matrix A, i.e. along which $\frac{dW}{ds}$ is always colinear with $r_m(W(s))$. Using the expression (23) of the right eigenvectors, it is easy to check that the following quantities are Riemann invariants:

m	1	2	3	4
λ_m	$u-c$	u	u	$u+c$
$\phi^{(m)}$	$u+\frac{2c}{\gamma(W)-1}$	u	u	$u-\frac{2c}{\gamma(W)-1}$
	$\frac{p}{\rho^{\gamma(W)}}$	p	p	$\frac{p}{\rho^{\gamma(W)}}$
	Y			Y

Table 1: Riemann invariants in the two-component case.

Several comments are needed here. Since Y is a Riemann invariant for the first and last characteristic field, Y is constant along a curve $W(s)$ parallel to the first or to the last eigenvector. This explains that the two other Riemann invariants for these fields are the same as in the single-component case. Beside this, there are only two Riemann invariants associated with the eigenvalue u because u is a double eigenvalue.

Once the Riemann invariants are known, the problem of evaluating the integral in (53) is essentially analogue to the similar problem in the single-component case, since Y (and therefore γ) is constant along those pieces of the integration path which are parallel to either r_1 or r_4. We refer the reader to [3] for more details. Again, two different Osher schemes can be defined, depending on the integration path between W_L and W_R.

3.4 A third multi-component extension: the approximate Riemann flux

A third approach ("approach (C)") is proposed in [15]; it is motivated by the observation that the above multi-component Roe and Osher schemes of type (B) do not preserve the maximum principle for the mass fraction (that is, these schemes do not preserve the inequalities $0 \leq Y \leq 1$; see Section 5 and Appendix A below). On the opposite the fully-coupled Van Leer schemes, and the fully-coupled Godunov scheme of Remark 3 do preserve the maximum principle for the mass fraction. It is shown in [15] that this property of the multi-component Godunov scheme is based on the following property of the exact solution of the Riemann problem (we use again the notation $\mathcal{W}$ of Remark 3):

Proposition 4:

For any states W_L and W_R, the following equality holds:

$$F^4[\mathcal{W}(0)] = F^1[\mathcal{W}(0)] \times \begin{cases} Y_L & \text{if } F^1[\mathcal{W}(0)] > 0\,, \\ Y_R & \text{if } F^1[\mathcal{W}(0)] < 0\,. \end{cases} \bullet \tag{55}$$

Therefore we define approach (C) as follows for the Roe and Osher schemes, where the flux evaluation is based on an approximate Riemann solver. We keep the first three components of $\phi_{i+1/2}$ evaluated as in approach (B), and we compute the fourth component $\phi^4_{i+1/2}$ of the flux from the next relation, which mimics (55):

$$\phi^4_{i+1/2} = \phi^1_{i+1/2} \times \begin{cases} Y^n_i & \text{if } \phi^1_{i+1/2} > 0 \ , \\ Y^n_{i+1} & \text{if } \phi^1_{i+1/2} < 0. \end{cases} \tag{56}$$

Therefore, we see from Proposition 4 that the Godunov scheme of type (B) is also of type (C). Approach (C) defines an approximate Riemann flux for the whole multi-component system, and uses the same discrete mass fluxes for the species equation and the continuity equation. But the main advantage of this approach it the following: it preserves the maximum principle for the mass fraction. The result shown in [15] is the following:

Proposition 5:

Under the following CFL-like conditions:

$$\frac{\Delta t}{\Delta x} \left[\frac{\max(\phi^1_{i+1/2}, 0)}{\rho^n_i} - \frac{\min(\phi^1_{i+1/2}, 0)}{\rho^n_{i+1}} \right] \leq 1 \ , \tag{57}$$

the schemes of type (C) preserve the maximum principle for the mass fraction Y: for all i and $n \geq 0$:

$$\min_j Y^0_j \leq Y^n_i \leq \max_j Y^0_j \ . \ \bullet \tag{58}$$

Remark 5: All our numerical experiments performed using the Roe of Osher schemes have shown that the condition (57) is not more restrictive in practice than the usual CFL condition. •

4 SECOND-ORDER ACCURATE UPWIND NUMERICAL SCHEMES

Let us now consider the second-order extensions of the preceding schemes. Starting from the previous first-order accurate schemes, the second-order accuracy will be obtained by using piecewise linear variables instead of piecewise constant variables, and by evaluating the fluxes $\phi_{i+1/2}$ at the half time step $n + 1/2$. We follow here the "MUSCL" approach of Van Leer [27]. The method involves six steps at each time level, starting from the values W^n_i:

(a) We evaluate slopes s^n_i for all variables which are chosen to be piecewise linear. Several choices are possible at this stage: for instance, one can choose either the conservative variables ρ, ρu, E, ρY or the "physical variables" ρ, u, p, Y, or also the characteristic variables (see [30]) to vary linearly in each computational cell.

(b) Slope limiters are used in order to avoid the creation of new extrema; here again different strategies exist to evaluate the limited slopes (see e.g. [6], [22], [25], [26]). In the numerical experiments whose results are reported below, we have used the superbee limiter of Roe [22].

(c) The limited slopes are used to evaluate cell-interface values $W^n_{i+1/2,\pm}$: for each piecewise linear variable f, one sets:

$$f^n_{i+1/2,-} = f^n_i + \frac{\Delta x}{2} s^n_i \ , \quad f^n_{i-1/2,+} = f^n_i - \frac{\Delta x}{2} s^n_i \ . \tag{59}$$

(d) The solution is advanced in time over a half time step using a centered predictor, setting:

$$W^{n+1/2}_i = W^n_i - \frac{\Delta t}{2\Delta x} \left[F(W_{i+1/2,-}) - F(W_{i-1/2,+}) \right] \ . \tag{60}$$

(e) Next, we again use the same slopes s^n_i to evaluate cell interface values $W^{n+1/2}_{i+1/2,\pm}$ at the half time step (we set $f^{n+1/2}_{i+1/2,-} = f^{n+1/2}_i + \frac{\Delta x}{2} s^n_i$).

(f) Lastly, we complete the time step by evaluating W^{n+1}_i, using the upwind numerical flux function Φ:

$$\frac{W^{n+1}_i - W^n_i}{\Delta t} + \frac{\phi^{n+1/2}_{i+1/2} - \phi^{n+1/2}_{i-1/2}}{\Delta x} = 0 \ , \tag{61}$$

where:

$$\phi^{n+1/2}_{i+1/2} = \Phi(W^{n+1/2}_{i+1/2,-}, W^{n+1/2}_{i+1/2,+}) \ . \tag{62}$$

This construction *(a)-(f)* can be applied to any multi-component numerical flux function Φ, that is to any of the schemes of types (A), (B) or (C) presented in the preceding sections.

Remark 6: It is shown in [15] that the second-order accurate schemes of type (C) preserve the maximum principle for the mass fraction when the slopes of the *physical* variables are limited, more precisely when the mass fraction Y itself (and not ρY) is among the variables which are chosen to vary linearly in each cell with limited slopes. •

Remark 7: We have restricted our attention to explicit first-order or second-order accurate schemes for the one-dimensional problem (13). But several further generalizations are possible: the extensions to N-component flows, to implicit schemes or to schemes operating on unstructured meshes for the simulation of multi-dimensional multi-component flows is straightforward (see e.g. [5], [15], [16]). •

5 NUMERICAL RESULTS AND COMPARISONS

We present in this section a detailed comparison of approaches (A), (B) and (C). For this purpose, we will mainly consider a two-component version of the classical shock tube problem of Sod [23]. In other words, we will solve the Riemann problem (26) with:

$$\begin{cases} \rho_L = 1\ , & \rho_R = 0.125\ , \\ u_L = 0\ , & u_R = 0\ , \\ p_L = 1\ , & p_R = 0.1\ . \end{cases} \tag{63}$$

The values of Y_L, Y_R, γ_L and γ_R may vary from one experiment to another and will be specified below. We will also sometimes consider a different (stiffer) shock-tube problem, where:

$$\begin{cases} \rho_L = 1\ , & \rho_R = 0.125\ , \\ u_L = 0\ , & u_R = 0\ , \\ p_L = 1000\ , & p_R = 1\ , \\ Y_L = 1\ , & Y_R = 0\ , \\ \gamma_L = 1.6\ , & \gamma_R = 1.4\ . \end{cases} \tag{64}$$

5.1 First-order accurate results

5.1.1 The Sod shock-tube with constant γ.

To begin with, we consider the first-order accurate solution of the Sod shock tube, with the same values of γ at both sides of the initial discontinuity: $\gamma_L = \gamma_R = 1.4$. Most results presented in this section will be presented for Roe scheme of type (A), (B) or (C), at time $t_0 = 0.21$. They have been obtained using 101 equally spaced grid points in the interval $[-0.5, 0.5]$, and 60 equal time steps (the average CFL number is around 0.75). The exact solution is also plotted on each Figure, together with the numerical solution.

When we use the uncoupled approach (A) (with the formulation (42) based on $\tilde{u}_{i+1/2}$), and with:

$$Y_L = 1\ ,\ \ Y_R = 0\ , \tag{65}$$

we obtain the mass fraction profiles shown on Figure 2 (the Figure shows both profiles of $Y_1 = Y$ and $Y_2 = 1 - Y$).

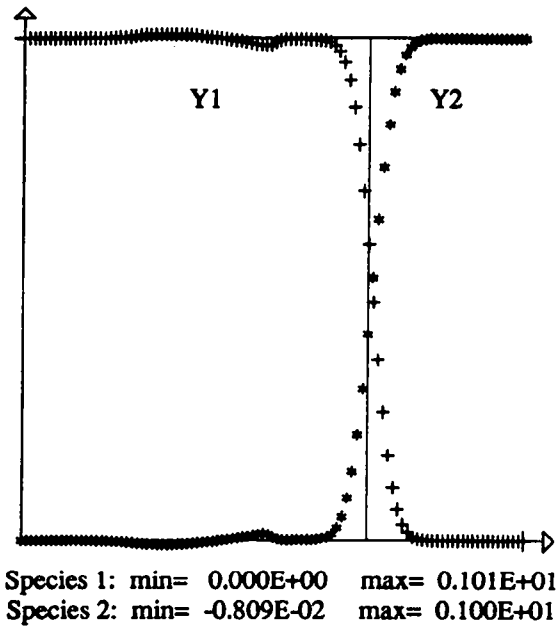

Figure 2: Mass fraction profiles for Sod shock tube with constant $\gamma = 1.4$ (first-order accurate Roe scheme (A), with initial data (65)).

With the same scheme, but with the initial data:

$$Y_L = 0 \ , \quad Y_R = 1 \ , \tag{66}$$

we obtain the profiles of Figure 3.

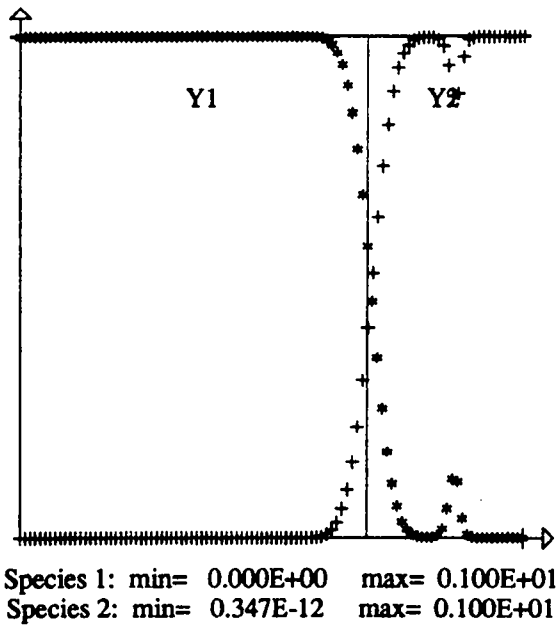

Figure 3: Mass fraction profiles for Sod shock tube with constant $\gamma = 1.4$ (first-order accurate Roe scheme (A), with initial data (66)).

We observe here that, althoug approach (A) preserves the positivity of Y, it gives very poor results. Oscillations appear in the rarefaction wave in Figure 2, whereas a "kink" appears at the forward propagating shock in Figure 3. In particular, unphysical mass fraction values exceeding 1 appear in Figure 2.

Another remark on these results concerns the comparisons of Figures 2 and 3. For the sake of clarity, let us call $\bar{Y}(x,t)$ the exact solution of the Riemann problem (26) with the data initial (63)-(65), and call $\hat{Y}(x,t)$ the exact solution of the Riemann problem (26) with the data initial (63)-(66). It is clear that these exact solutions satisfy the relation:

$$\bar{Y}(x,t) + \hat{Y}(x,t) \equiv 1 \ . \tag{67}$$

But Figures 2 and 3 show that the analogous relation is far from being true for the mass fractions computed with approach (A). In other words, calling Σ_1 or Σ_2 the gaseous species which is initially in the left compartment of the shock tube has an influence on the numerical results ! This surprising fact comes from the conservative formulation: the mass fraction

is obtained as a *nonlinear* function of the dependent variables: $Y = \frac{W_4}{W_1}$. This is also the reason why approach (A) behaves so badly (there is indeed no need to say that the schemes of type (A) derived from the Osher and Van Leer schemes or from (40) also perform poorly): the mass fraction is evaluated as the ratio of two variables which are advanced in time using two different approximations, or more precisely two different upwindings: the upwinding for W_1 is based on the artificial viscosity of Roe scheme, while the upwinding for W_4 is based on the donor-cell formulation (40) or (42).

We can also explain why the oscillations do not appear in the rarefaction wave in Figure 3, or why the kink does not appear at the shock in Figure 2. Obviously from the donor-cell formulation (40) or (42), the scheme behaves correctly where $Y \equiv 0$: if $Y_{j-1}^n = Y_j^n = Y_{j+1}^n = 0$, then $Y_j^{n+1} = 0$. But if we consider a problem where Y does not vanish, we get at the same time the oscillations in the rarefaction wave and the kink at the shock (see Figure 4 where we have taken $Y_L = 0.75$, $Y_R = 0.25$).

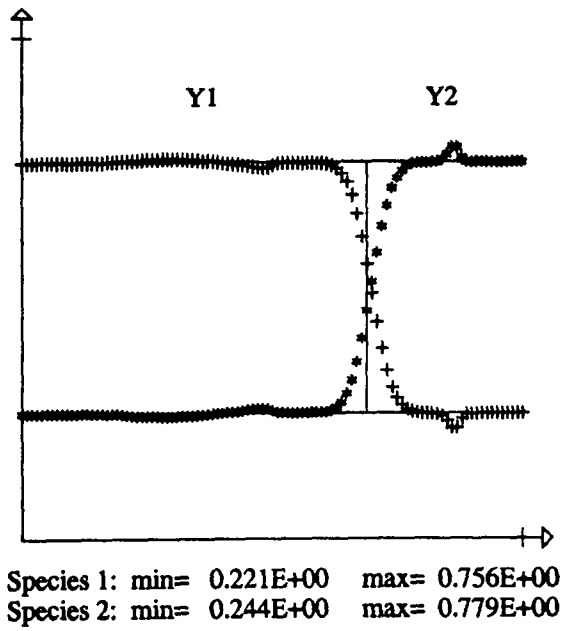

Figure 4: Mass fraction profiles for Sod shock tube with constant $\gamma = 1.4$ (first-order accurate Roe scheme (A), with $Y_L = 0.75$, $Y_R = 0.25$).

Therefore, approach (A) gives unacceptable results; we will not consider it any longer.

In contrast with the preceding results, approach (B) gives much better mass fraction profiles. For the same problem as in Figure 2, we obtain the results of Figure 5. Clearly, the discontinuity is smeared by the numerical diffusion, which is rather strong here since we use a first-order accurate scheme; we can also note that some computed values of Y lie outside the interval $[0, 1]$. Nevertheless, the results are very acceptable.

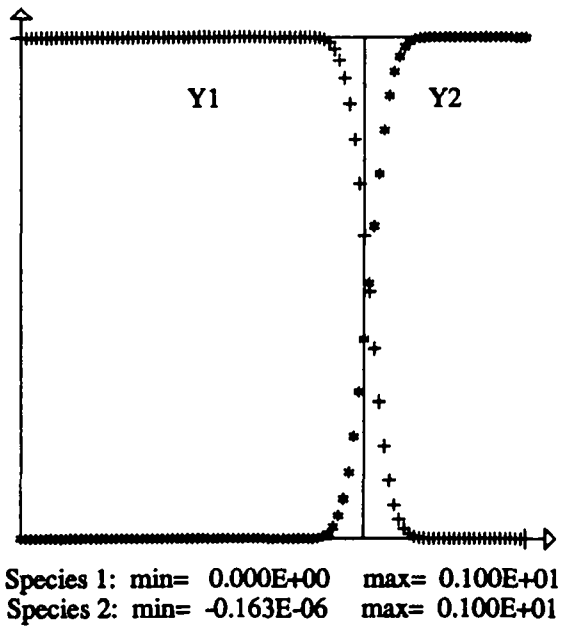

Figure 5: Mass fraction profiles for Sod shock tube with constant $\gamma = 1.4$ (first-order accurate Roe scheme (B), with initial data (65)).

Another progress in comparison with approach (A) is the following: if we consider the problem with initial data (66) (that is, if we change left and right), we obtain the profiles of Figure 6, which look very close to those of Figure 5. In fact, in this particular case where γ is constant, one can prove that the identity (67) is preserved in approach (B) (using the relations (70)-(71), (75)-(76) and (80)-(81) in Appendix A).

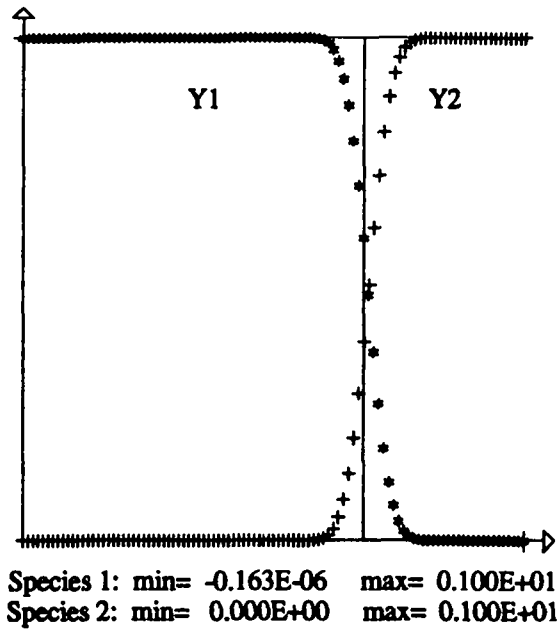

Figure 6: Mass fraction profiles for Sod shock tube with constant $\gamma = 1.4$ (first-order accurate Roe scheme (B), with initial data (66)).

Lastly, we consider the Roe scheme of type (C). The computed mass fraction profiles are very similar to the ones obtained in approach (B), although now the computed values of the mass fraction remain in the interval $[0, 1]$, as expected from Proposition 5 (see Figure 7). Moreover, approach (C) also preserves the identity (67): exchanging the roles of Y_L and Y_R has no influence on the results.

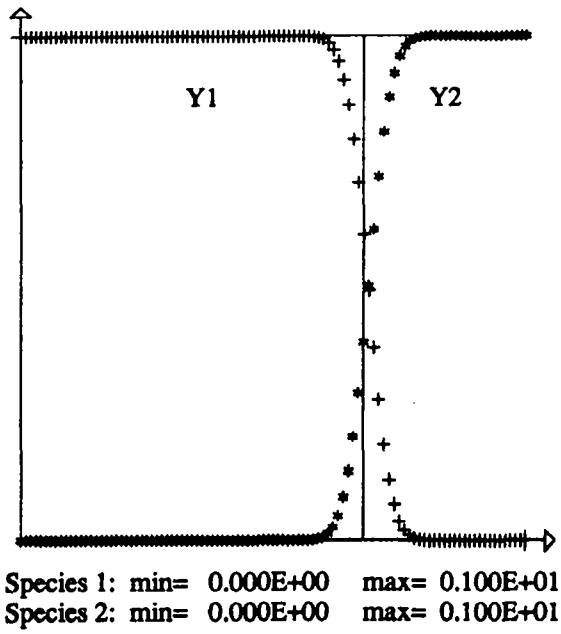

Figure 7: Mass fraction profiles for Sod shock tube with constant $\gamma = 1.4$ (first-order accurate Roe scheme (C), with initial data (65)).

For the sake of completeness, we conclude this paragraph by showing the results obtained for the hydrodynamic variables ρ, u, p and for the Mach number $\mathcal{M}$. In fact, these results are classical, since it is easy to see that, in this case where γ is constant, that is where there is no influence of the mass fraction Y over the flow, all approaches (A), (B) or (C) give the same results for all hydrodynamic variables ρ, u, p, T, $\cdots$, which is also the same result as given by the numerical solution of the classical single-component Sod shock tube. Thus, the slight differences between the solutions of the Roe, Van Leer, Osher-Solomon or "physical Osher" schemes have already been observed in the literature (see e.g. [8], [28], and Figures 8 to 11).

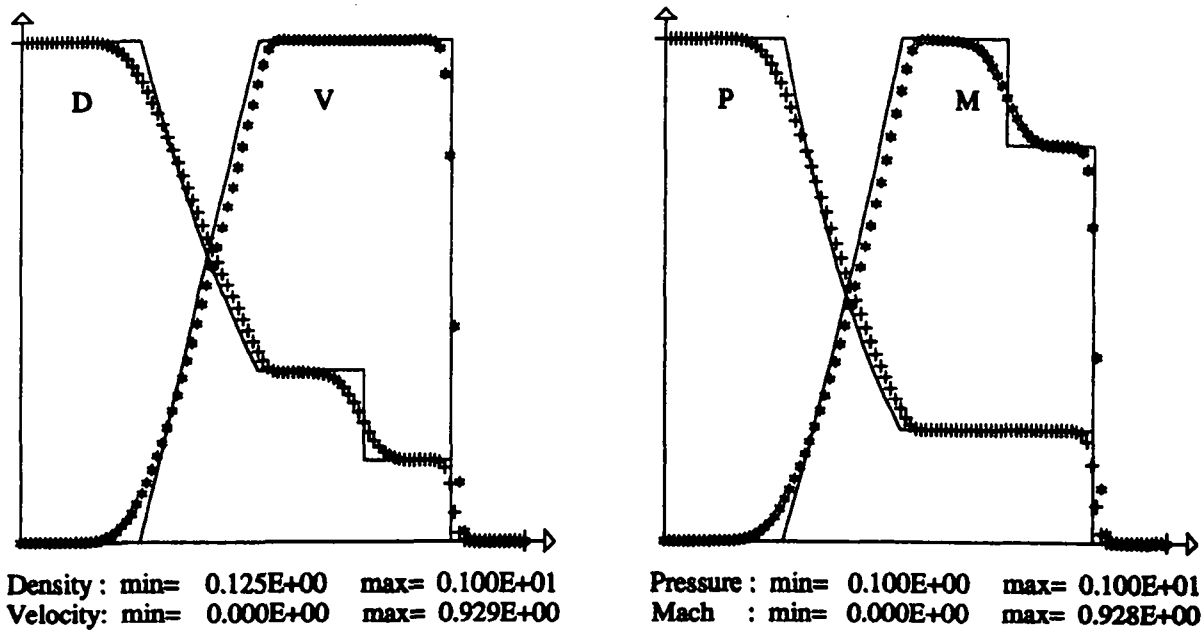

Figure 8: Density, velocity, pressure and Mach number profiles for Sod shock tube with constant $\gamma = 1.4$ (first-order accurate Roe scheme).

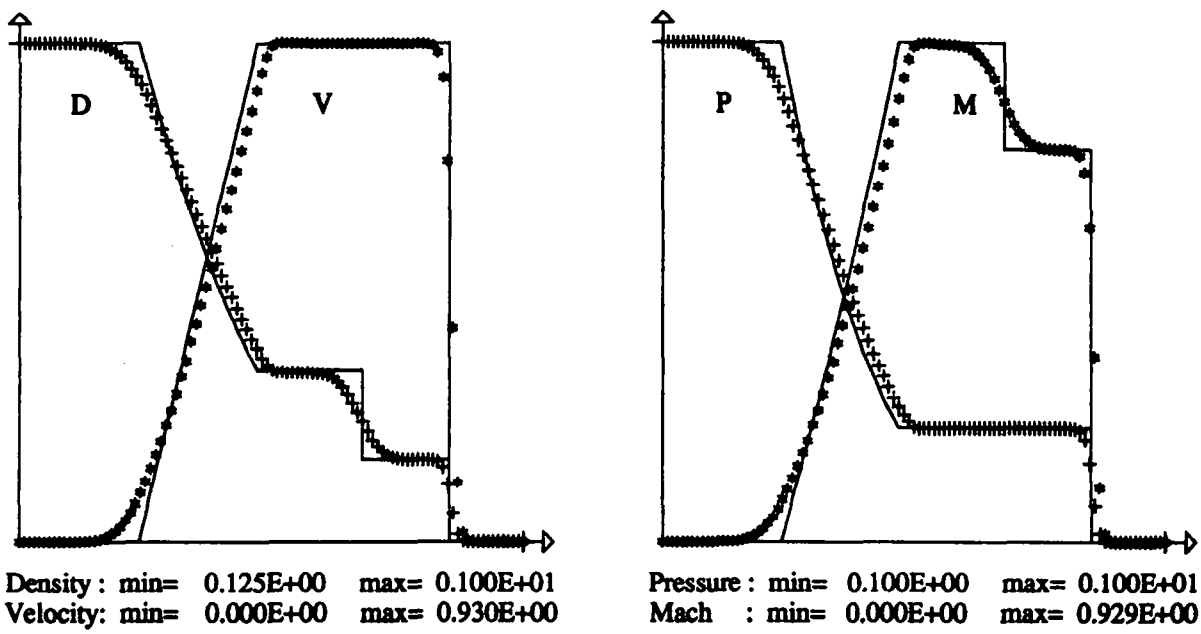

Figure 9: Density, velocity, pressure and Mach number profiles for Sod shock tube with constant $\gamma = 1.4$ (first-order accurate Osher-Solomon scheme).

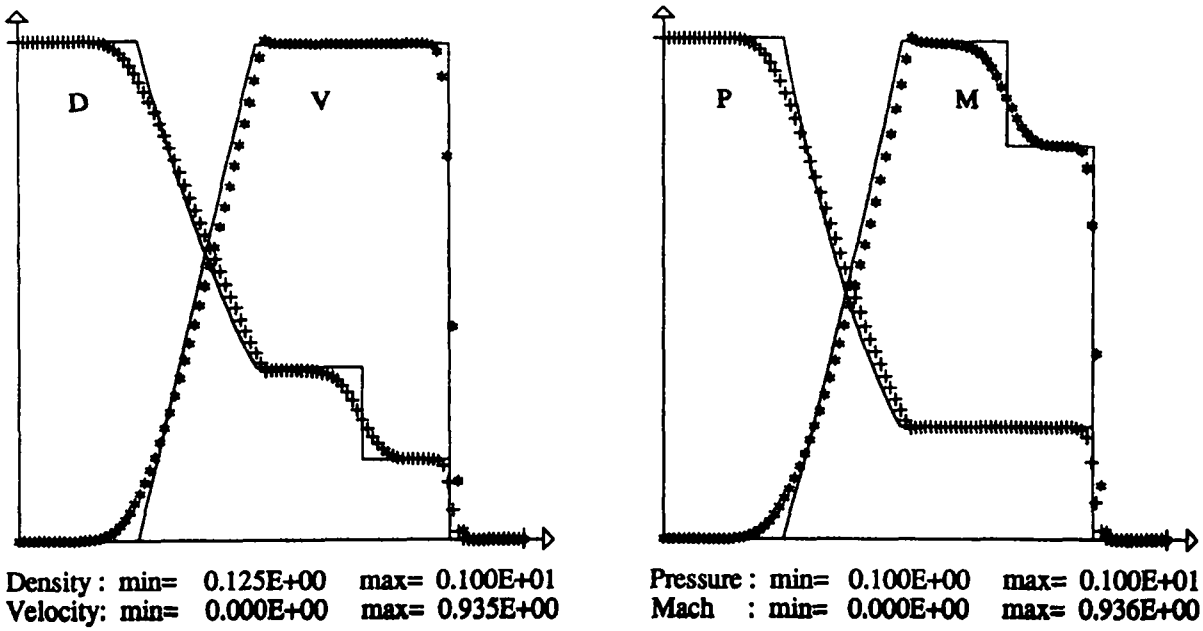

Figure 10: Density, velocity, pressure and Mach number profiles for Sod shock tube with constant $\gamma = 1.4$ (first-order accurate "physical Osher" scheme).

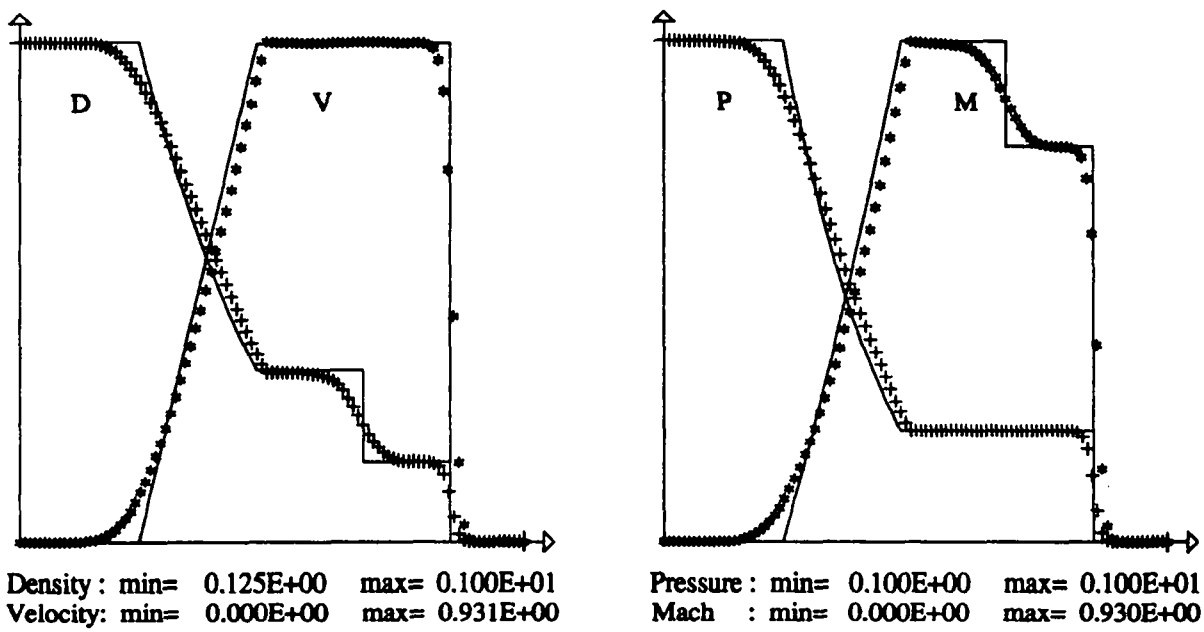

Figure 11: Density, velocity, pressure and Mach number profiles for Sod shock tube with constant $\gamma = 1.4$ (first-order accurate Van Leer scheme).

5.1.2 The Sod shock tube with variable γ

We now solve the Sod shock tube problem with non constant γ: we take $\gamma_L = 1.4$, $\gamma_R = 1.2$, and $Y_L = 1$, $Y_R = 0$.

The results are shown on Figures 12 to 18 for the multi-component Van Leer scheme (B) and for the multi-component extensions (B) or (C) of the three schemes of Roe, Osher-Solomon and "physical Osher".

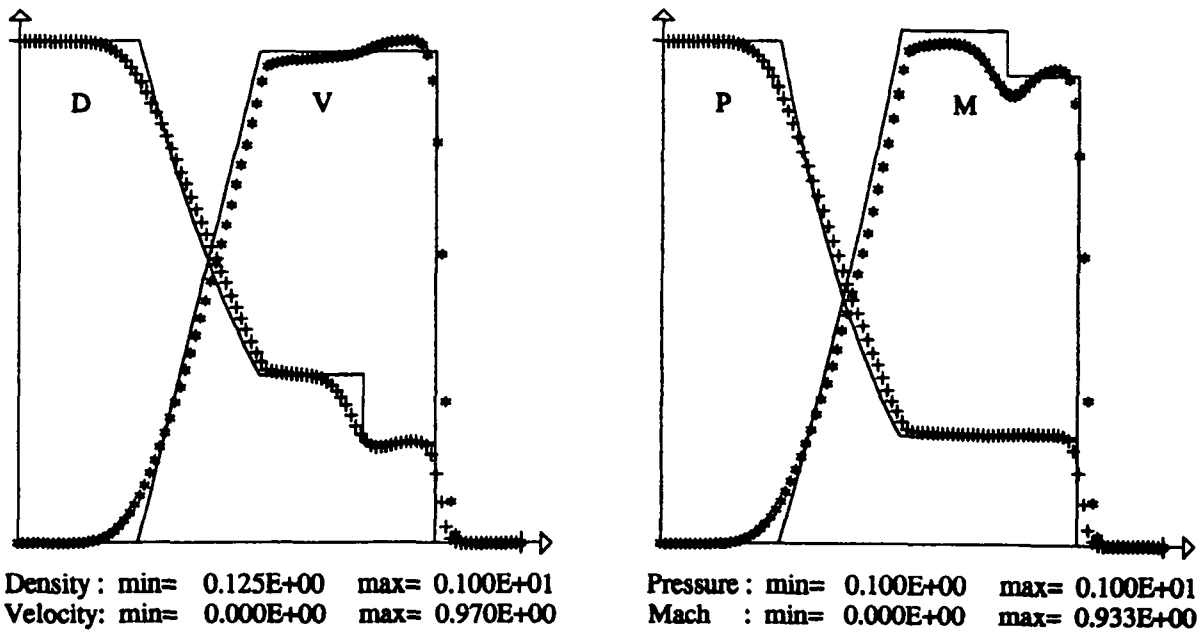

Figure 12: Density, velocity, pressure and Mach number profiles for Sod shock tube with variable γ (first-order accurate Van Leer scheme (B)).

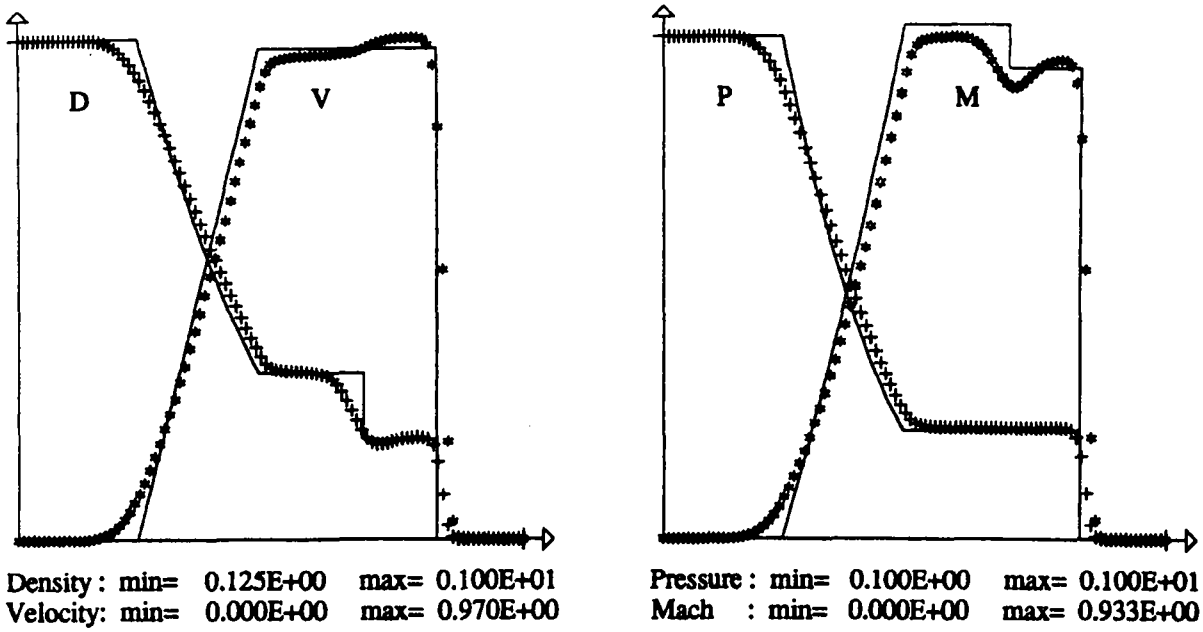

Figure 13: Density, velocity, pressure and Mach number profiles for Sod shock tube with variable γ (first-order accurate Roe scheme (B)).

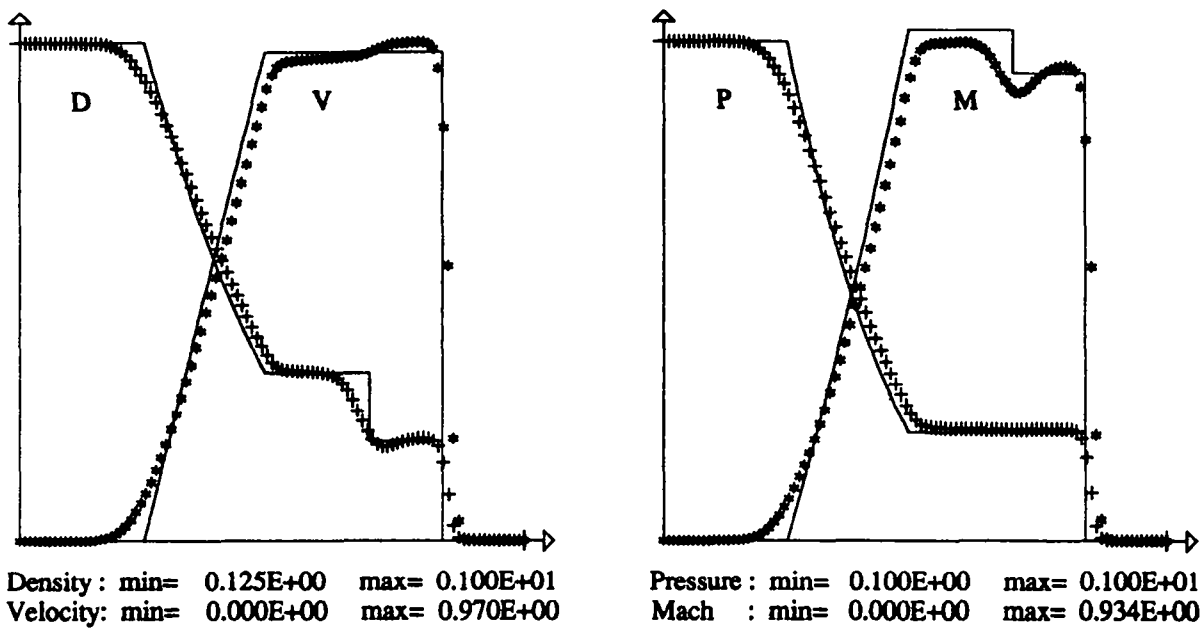

Figure 14: Density, velocity, pressure and Mach number profiles for Sod shock tube with variable γ (first-order accurate Roe scheme (C)).

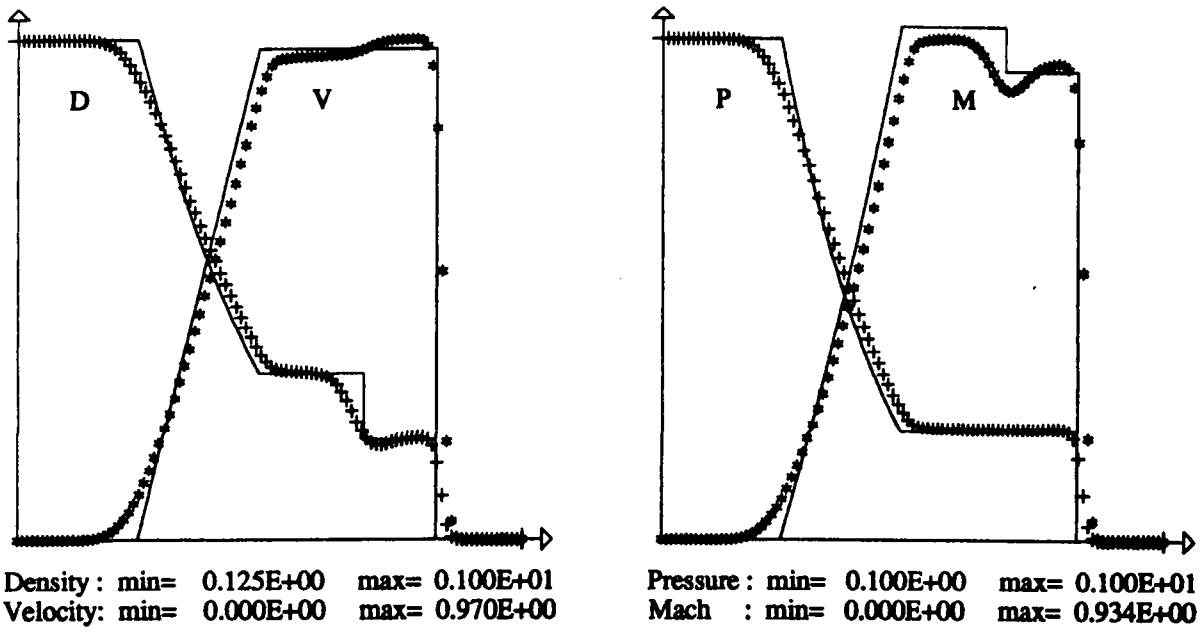

Figure 15: Density, velocity, pressure and Mach number profiles for Sod shock tube with variable γ (first-order accurate Osher-Solomon scheme (B)).

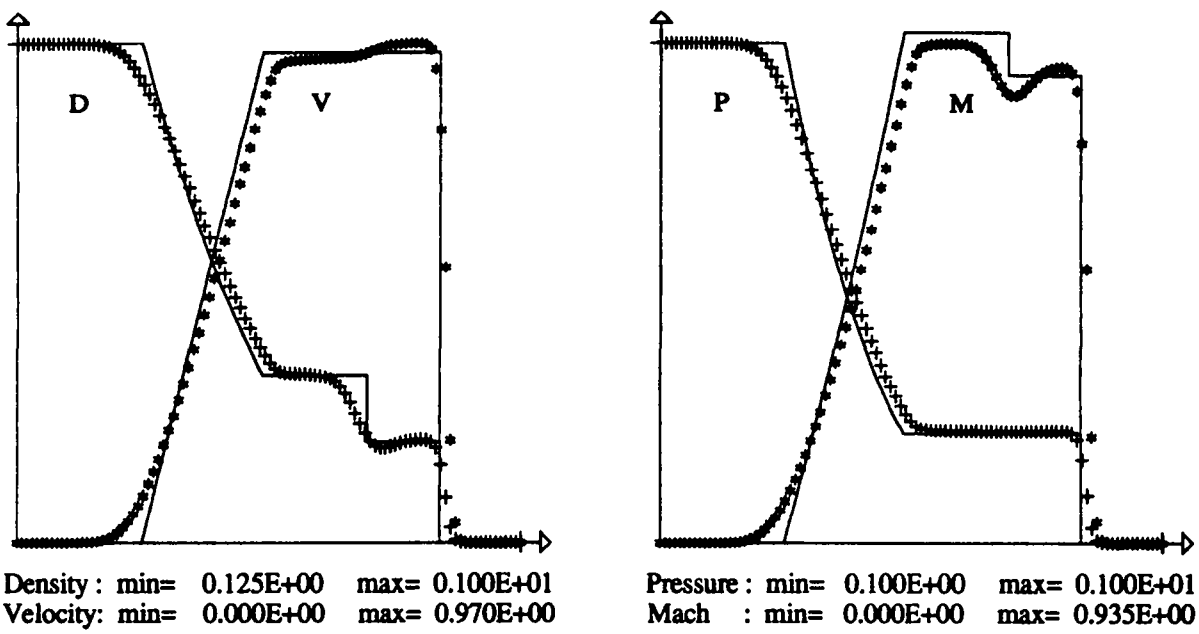

Figure 16: Density, velocity, pressure and Mach number profiles for Sod shock tube with variable γ (first-order accurate Osher-Solomon scheme (C)).

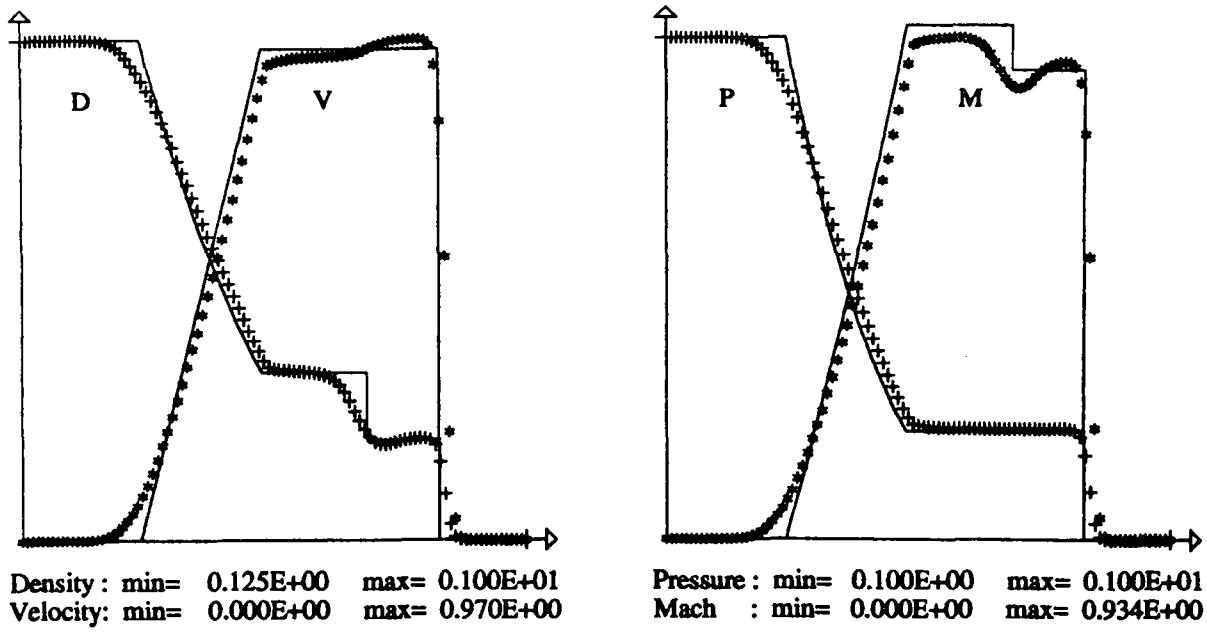

Figure 17: Density, velocity, pressure and Mach number profiles for Sod shock tube with variable γ (first-order accurate "physical Osher" scheme (B)).

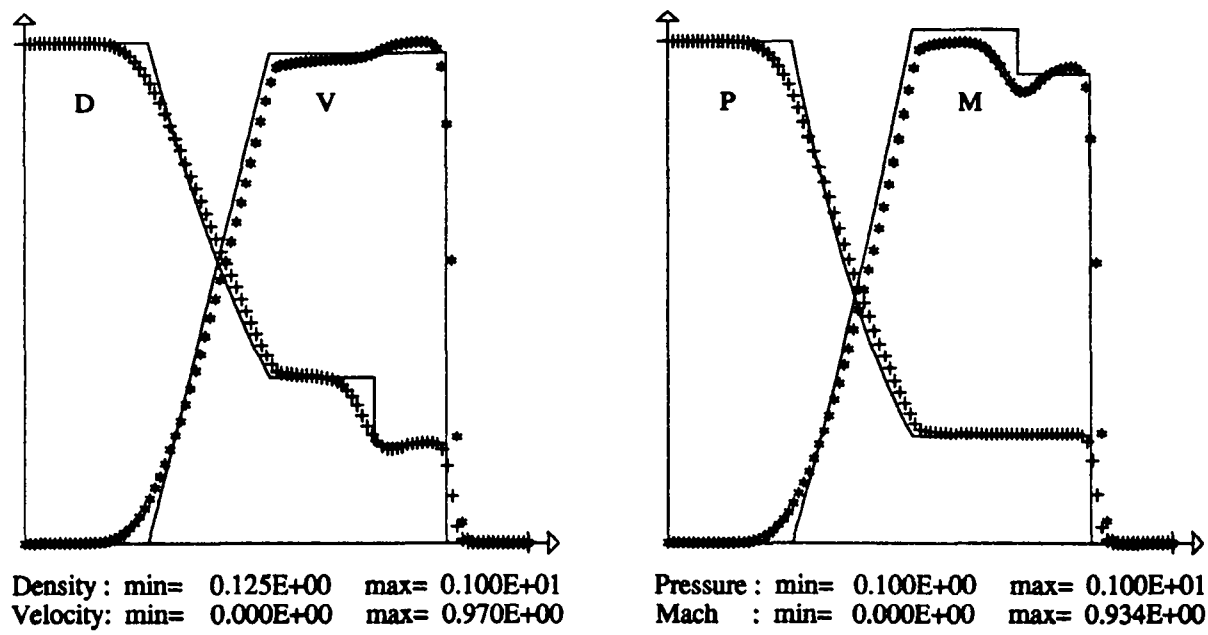

Figure 18: Density, velocity, pressure and Mach number profiles for Sod shock tube with variable γ (first-order accurate "physical Osher" scheme (C)).

An interesting difference between these results and those obtained with constant γ in Figures 8 to 11 is the discontinuity of the velocity which appears at the contact discontinuity. Clearly, this phenomenon is due to the fact that γ is no longer constant in the present results; an analysis of this point is presented in Appendix B below.

Apart from this, we again observe on Figures 12 to 18 some slight differences between the results provided by the different schemes. But the major conclusion here is that no significant difference can be observed between the fully coupled schemes (B) and schemes (C).

Only for the mass fraction profiles can we find a real qualitative difference between approaches (B) and (C), since the computed values of Y always lie in the interval $[0, 1]$ when approach (C) is used, whereas minimal values of Y of the order of -10^{-6} are obtained with the Roe and Osher schemes of type (B) (the calculations use double-precision arithmetics). We do not show here the mass fraction profiles, since they all look very close to those of Figures 5 to 7.

We can also compare the costs of approaches (B) and (C). In the above experiments, the multi-component Roe, Osher-Solomon and "physical Osher" schemes of type (C) appeared to be about 8% cheaper than the corresponding scheme of type (B). We can also add here that this efficiency of approach (C) relative to approach (B) would be even greater if more than two species were involved in the gaseous mixture under consideration.

5.1.3 The approach (C) with frozen γ

As it was proposed in a preliminary version of [15], we could also consider a simplified approach (C), with the first three components of the flux $\phi_{i+1/2}$ evaluated *as in approach (A), with a frozen* γ, and the fourth component $\phi^4_{i+1/2}$ evaluated from (56). This intermediate approach would therefore have the programming simplicity of approach (A), but would nevertheless use the property (56) of the multi-component Riemann flux, which in particular guarantees the preserving of the maximum principle for the mass fraction.

The results are shown on Figure 19, for the Roe scheme of type (C) with frozen γ, on the Sod shock tube problem with variable γ. Clearly these results are worse than those of the true approach (C) shown in Figure 13, especially in the neighbourhood of the contact discontinuity. The gain in CPU time is another 8%.

It is interesting to notice here that this difference between approaches (B) and (C) on one side and approach (C) with frozen γ on the other side is appreciably reduced when we solve the stiffer shock tube (64) instead of Sod shock tube. An explanation for this fact can be found in the expression (50) of the Roe matrix $\tilde{A}$. Freezing γ essentially amounts to neglecting X in the first term of the second and third rows of $\tilde{A}$: therefore, the bigger the ratio $\dfrac{X}{u^2}$, the bigger the numerical error due to freezing γ. But a rough evaluation of this ratio shows that $\dfrac{X}{u^2} \simeq 3$ for Sod shock tube, whereas $\dfrac{X}{u^2} \simeq 10^{-3}$ for the stiffer shock tube.

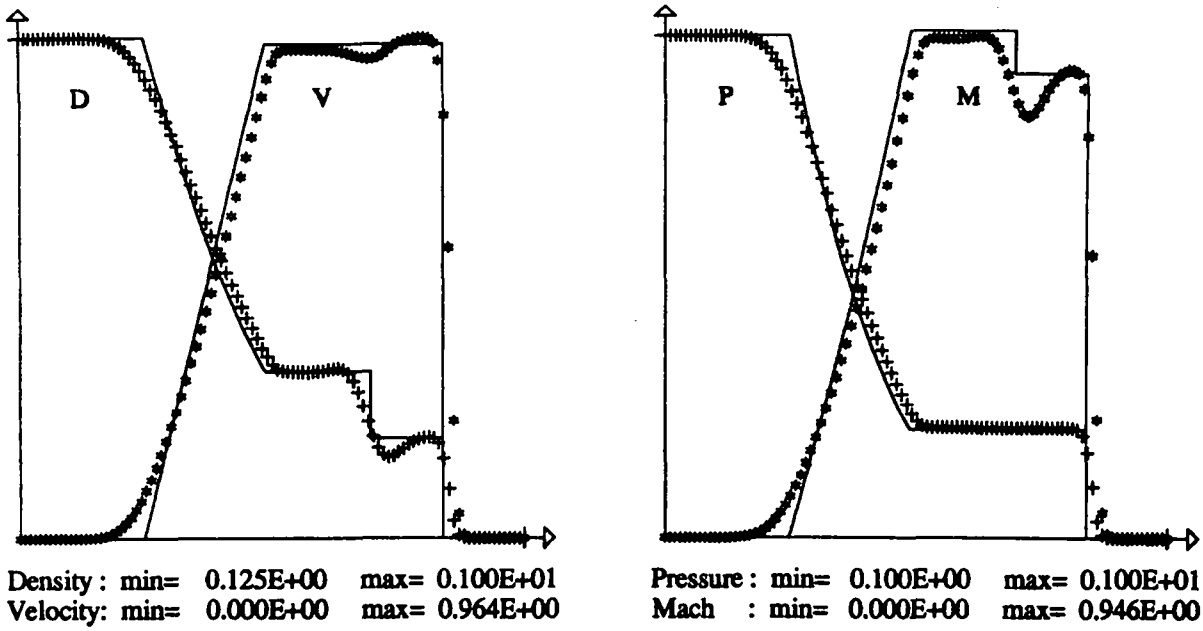

Figure 19: Density, velocity, pressure and Mach number profiles for Sod shock tube with variable γ (first-order accurate Roe scheme (C) with frozen γ).

The results for the stiffer shock tube are shown of Figures 20 to 22. Again no noticeable difference is observed between approaches (B) and (C) (except again for the mass fractions, where values of the order of -10^{-6} again appear in approach (B)); but the results obtained with γ frozen are more acceptable in this case.

Nevertheless, we will not consider any longer this simplified approach (C) with γ frozen in the sequel; the true approach (C) is undoubtedly preferable.

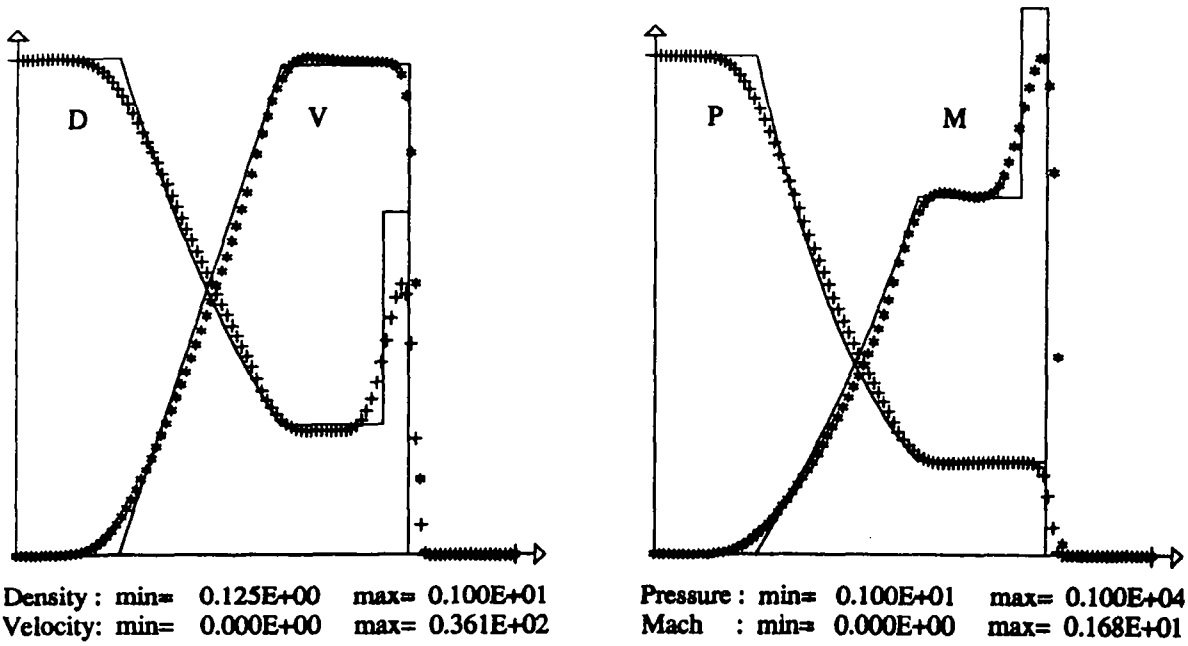

Figure 20: Density, velocity, pressure and Mach number profiles for the stiffer shock tube (64) with variable γ (first-order accurate Roe scheme (B)).

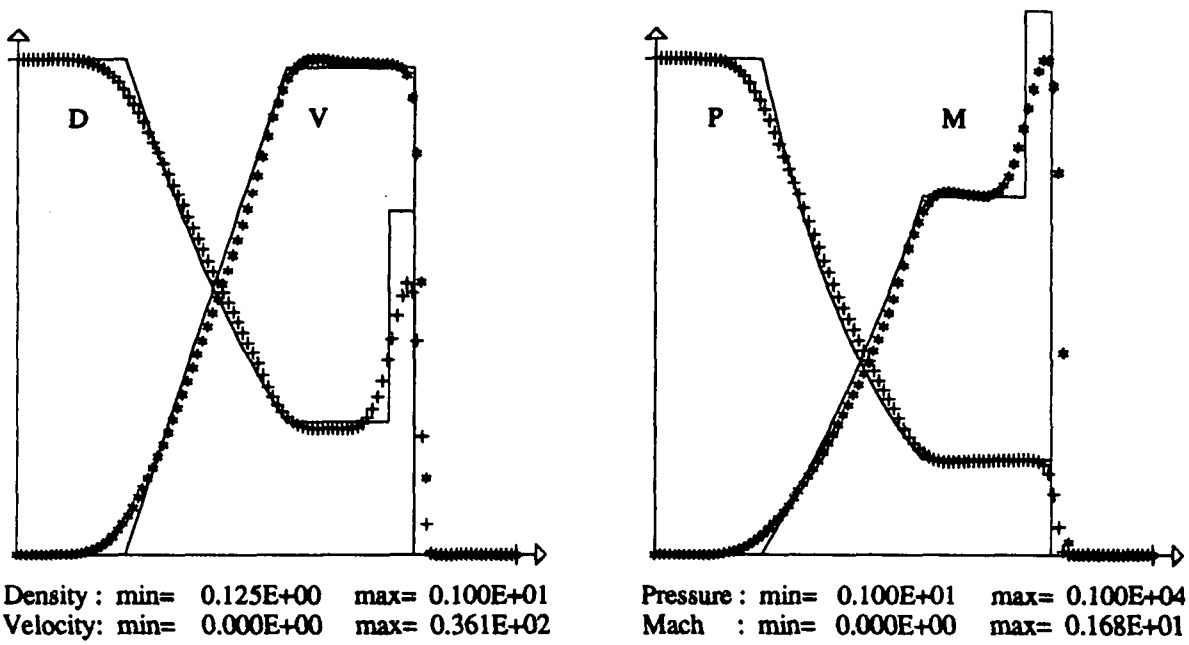

Figure 21: Density, velocity, pressure and Mach number profiles for the stiffer shock tube (64) with variable γ (first-order accurate Roe scheme (C)).

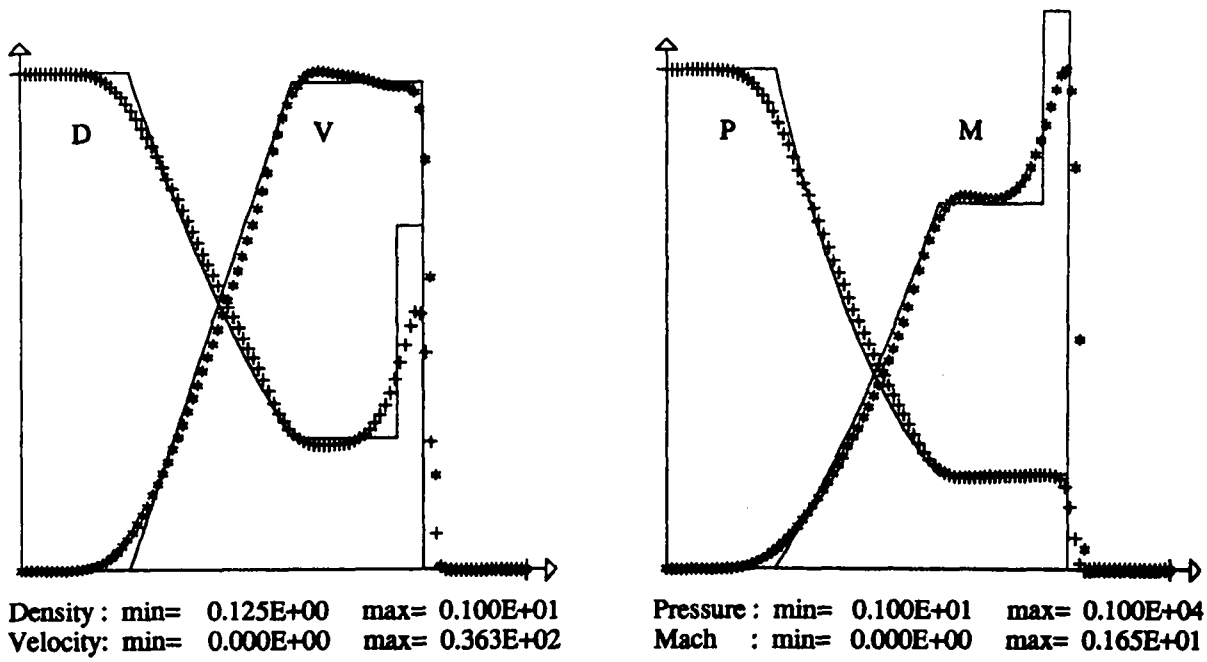

Figure 22: Density, velocity, pressure and Mach number profiles for the stiffer shock tube (64) with variable γ (first-order accurate Roe scheme (C) with frozen γ).

5.2 Second-order accurate results

5.2.1 The Sod shock tube with constant γ

We now consider the second-order accurate solution of the Sod shock tube with the intial data (65) and $\gamma_L = \gamma_R = 1.4$. Since γ is constant, the results given in this case by schemes (B) and (C) for the hydrodynamical variables coincide with the corresponding results for the single-component Sod shock tube. Nevertheless, we show them below for the sake of completeness.

Figure 23 shows the mass fraction profiles obtained with the second-order accurate Roe scheme of type (C). In this result, as in all other second-order accurate calculations, the width of the numerically smeared contact discontinuity has been reduced by a factor of about 2 in comparison with the first-order accurate of Figures 5 to 7 (of course, the mesh and time step have not been changed).

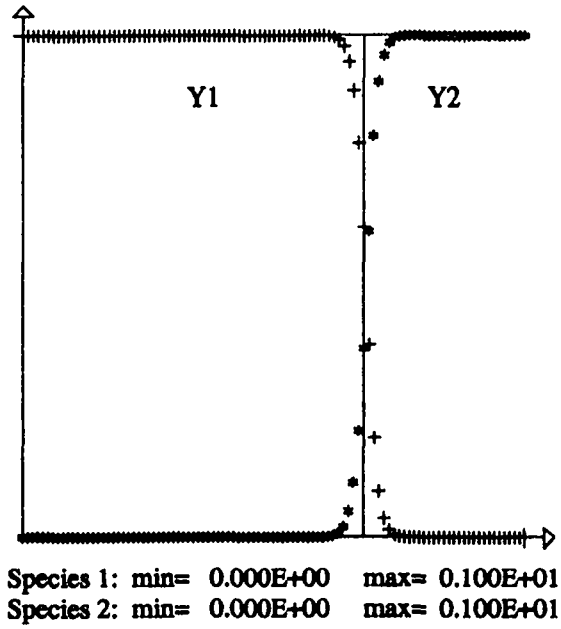

Figure 23: Mass fraction profiles for Sod shock tube with constant $\gamma = 1.4$ (second-order accurate Roe scheme (C), limiters acting on the physical variables).

No noticeable difference appears between the mass fraction profiles given by the various second-order accurate schemes under consideration, except that the values of Y evaluated using the Roe and Osher schemes (B) range in the interval $[-10^{-3}, 1]$, irrespective of whether the slope limiters are applied to the conservative, physical or characteristic variables, whereas the Van Leer scheme (with any limiting strategy) and the schemes (C) with the limiters acting on the physical variables do preserve the maximum principle for the mass fraction (as expected from Remark 6).

The results for the hydrodynamical variables are shown on Figures 24 to 32 for the Roe, Osher-Solomon and Van Leer schemes, with the three different limiting strategies. We reach here the same conclusions as in the single-component case: the results obtained when limiting the conservative variables are worse than those obtained when limiting the physical variables, which are in turn slightly worse than those obtained with the limiters acting on the characteristic variables (the costs of these three strategies are of course in the opposite order). We do not show the results obtained with the "physical Osher" scheme, which are close to those of the Roe and Osher-Solomon scheme.

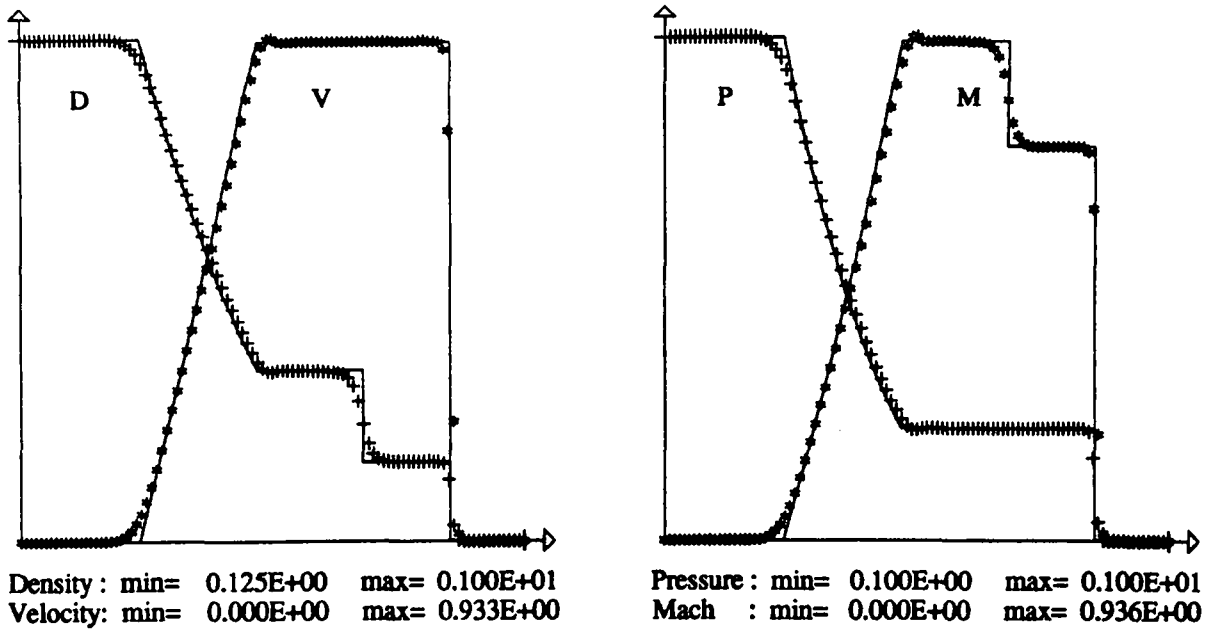

Figure 24: Density, velocity, pressure and Mach number profiles for Sod shock tube with constant $\gamma = 1.4$ (second-order accurate Roe scheme, limiters acting on the conservative variables).

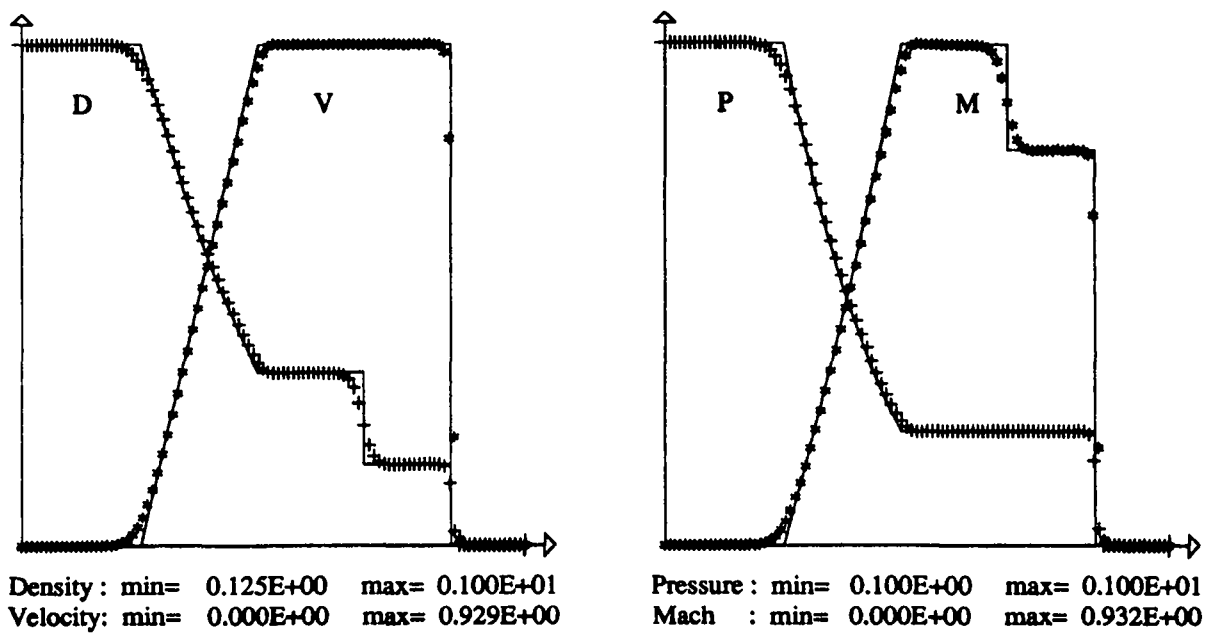

Figure 25: Density, velocity, pressure and Mach number profiles for Sod shock tube with constant $\gamma = 1.4$ (second-order accurate Roe scheme, limiters acting on the physical variables).

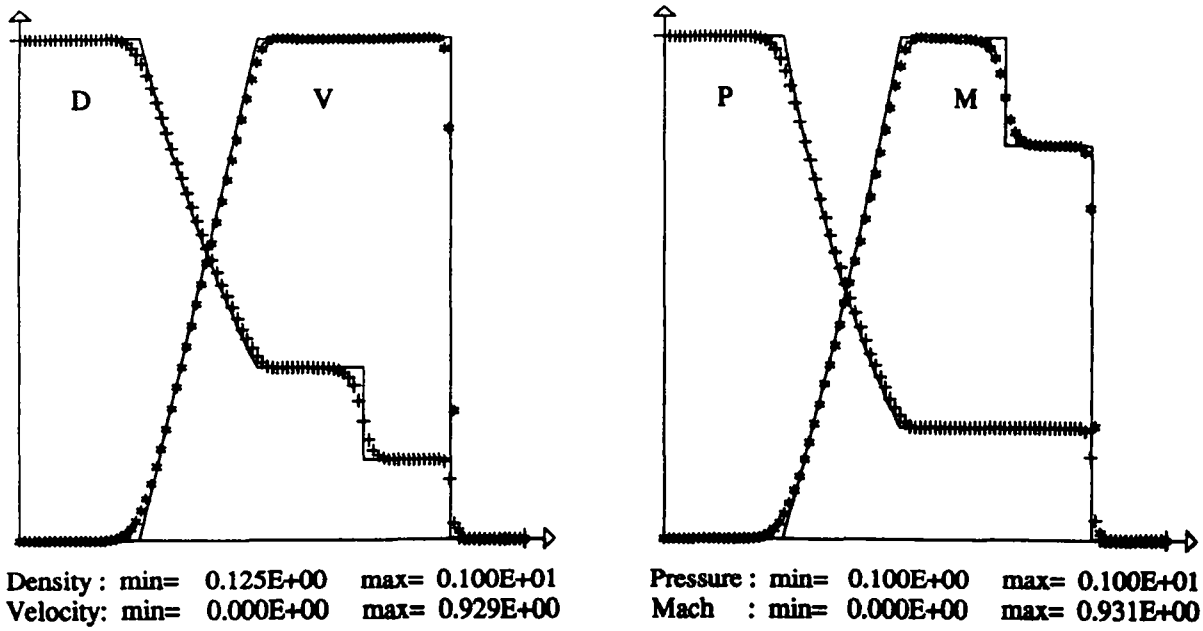

Figure 26: Density, velocity, pressure and Mach number profiles for Sod shock tube with constant $\gamma = 1.4$ (second-order accurate Roe scheme, limiters acting on the characteristic variables).

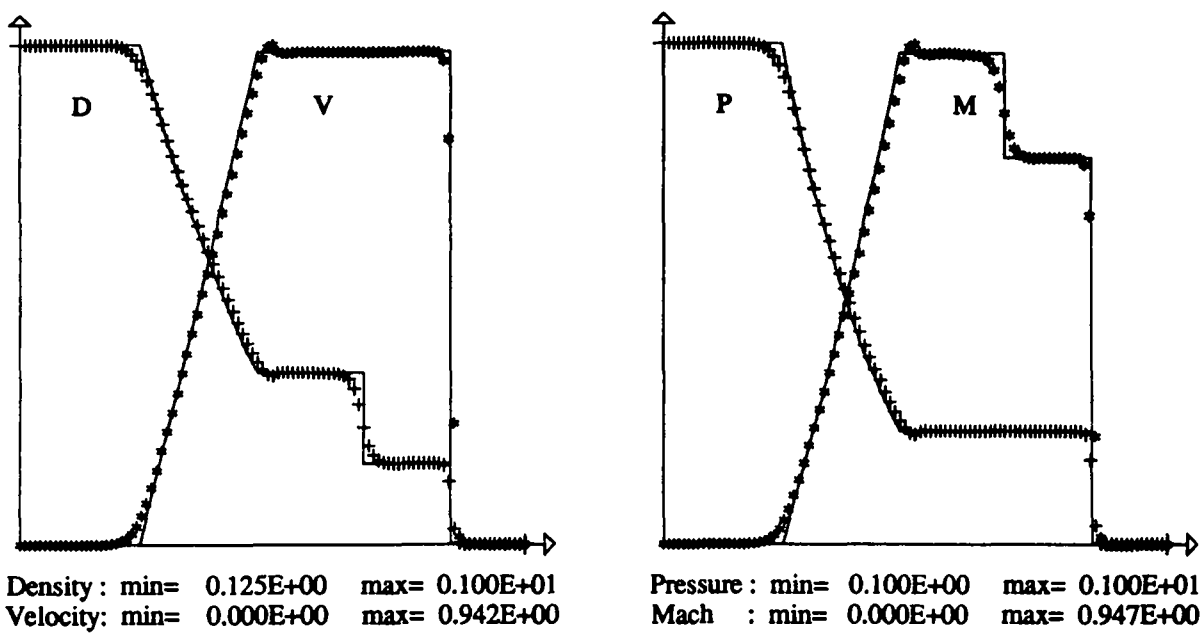

Figure 27: Density, velocity, pressure and Mach number profiles for Sod shock tube with constant $\gamma = 1.4$ (second-order accurate Osher-Solomon scheme, limiters acting on the conservative variables).

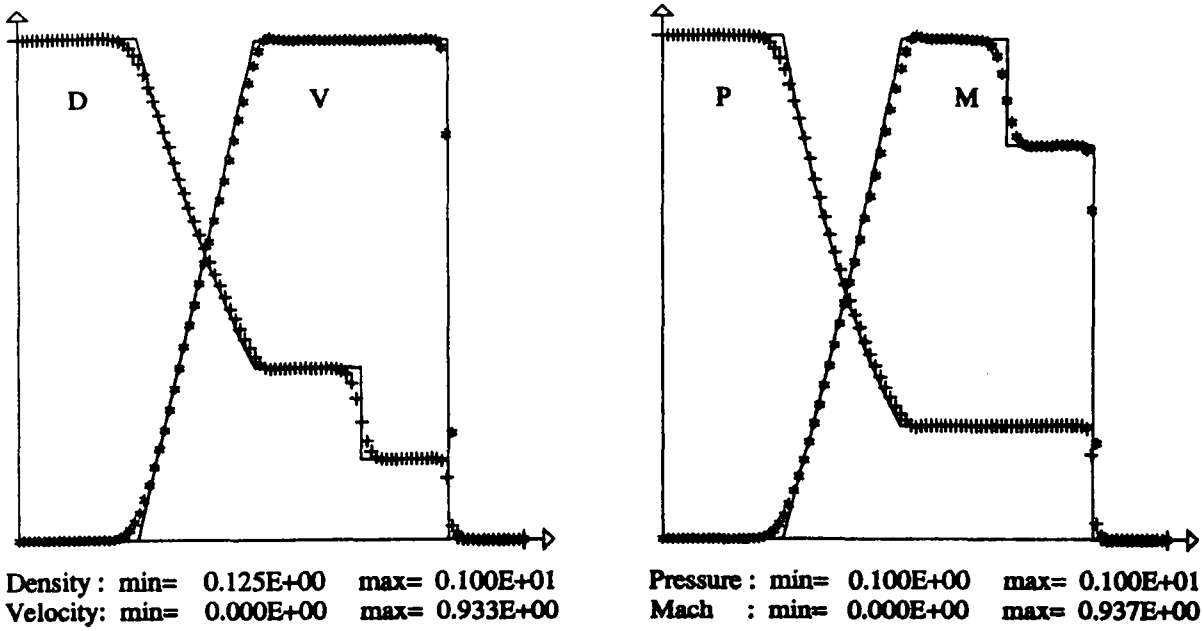

Figure 28: Density, velocity, pressure and Mach number profiles for Sod shock tube with constant $\gamma = 1.4$ (second-order accurate Osher-Solomon scheme, limiters acting on the physical variables).

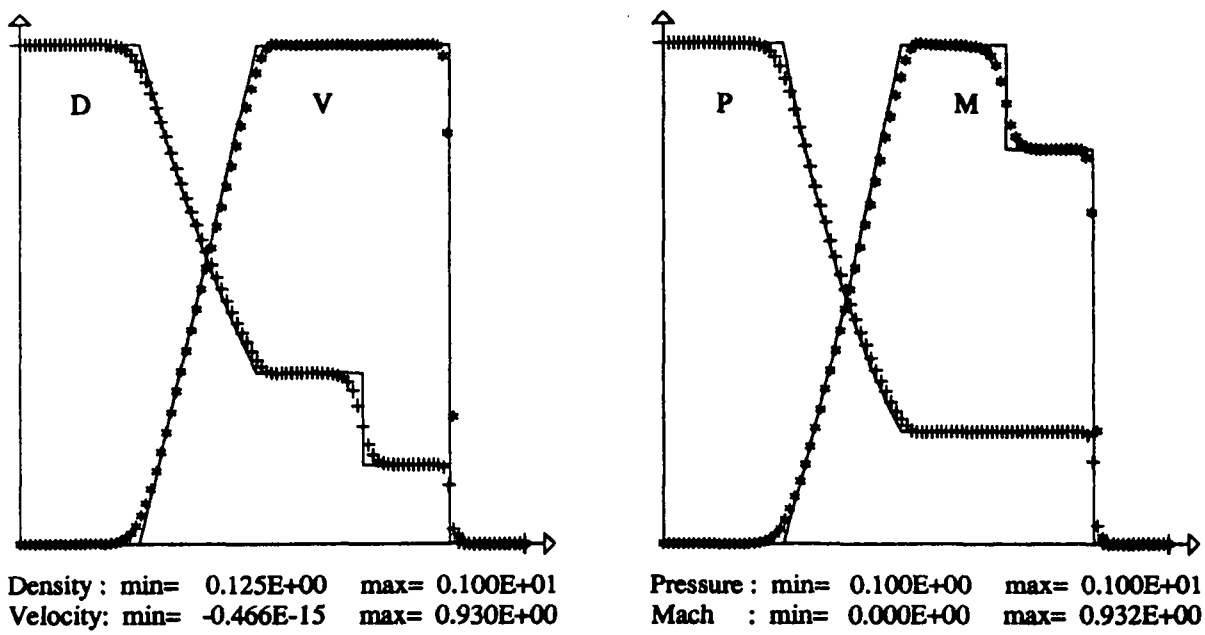

Figure 29: Density, velocity, pressure and Mach number profiles for Sod shock tube with constant $\gamma = 1.4$ (second-order accurate Osher-Solomon scheme, limiters acting on the characteristic variables).

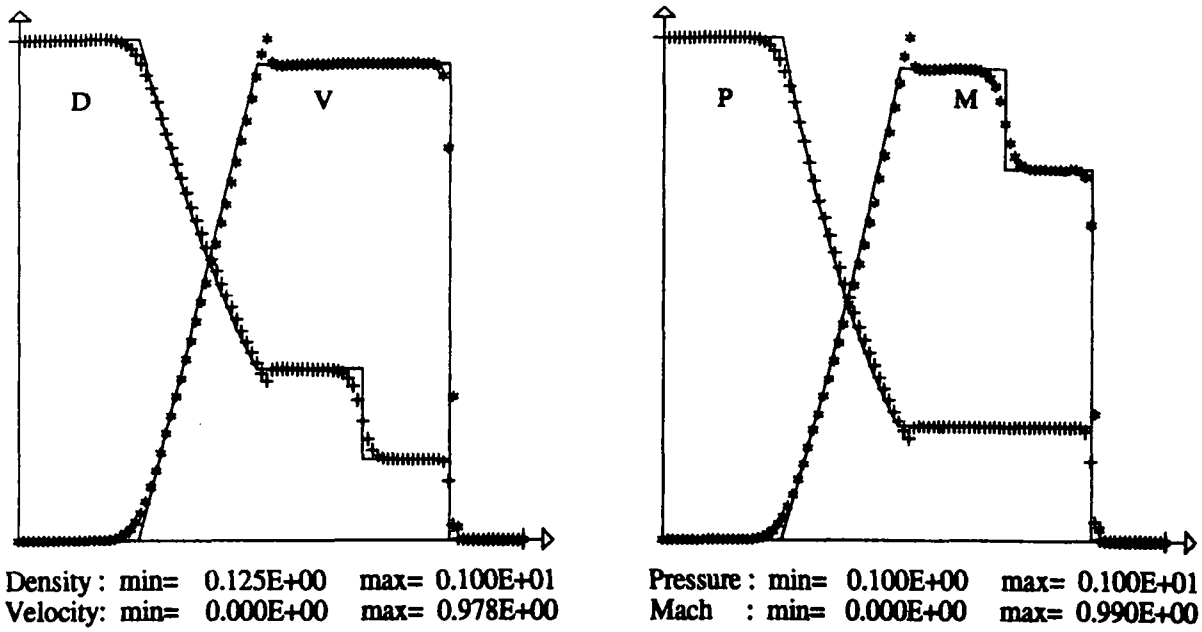

Figure 30: Density, velocity, pressure and Mach number profiles for Sod shock tube with constant $\gamma = 1.4$ (second-order accurate Van Leer scheme, limiters acting on the conservative variables).

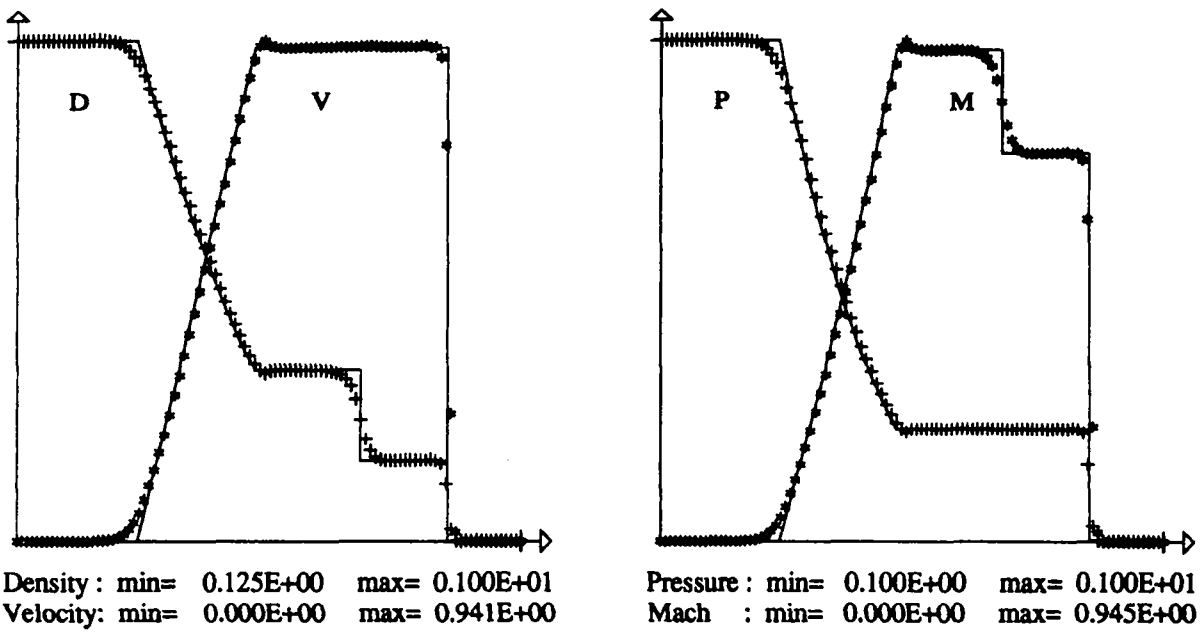

Figure 31: Density, velocity, pressure and Mach number profiles for Sod shock tube with constant $\gamma = 1.4$ (second-order accurate Van Leer scheme, limiters acting on the physical variables).

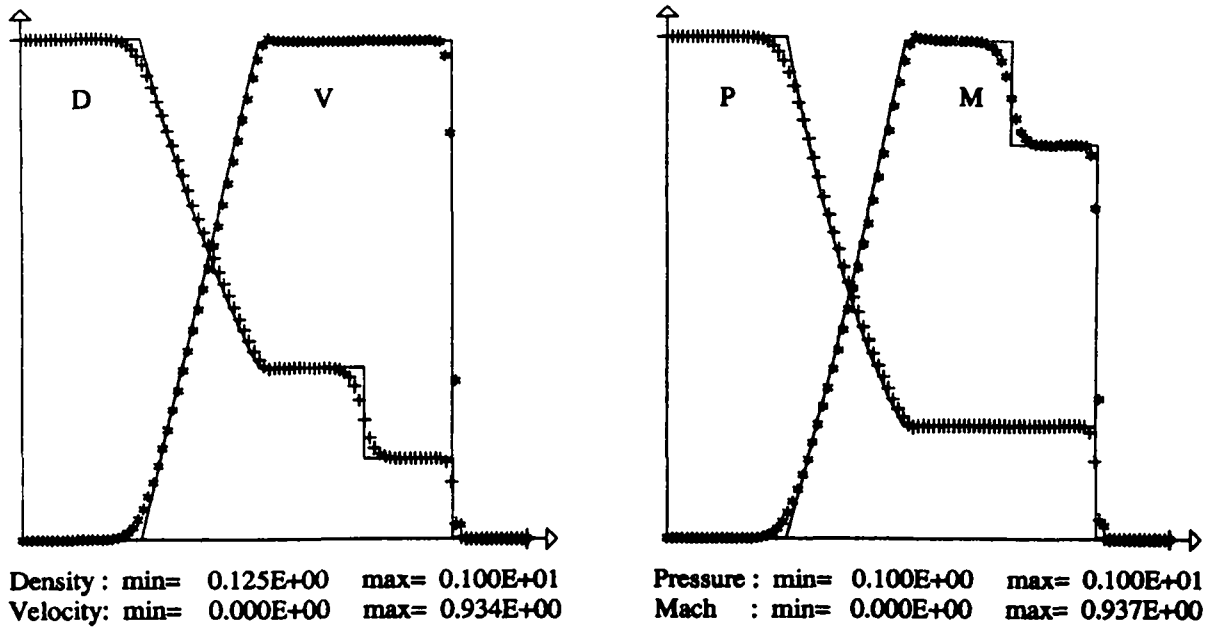

Figure 32: Density, velocity, pressure and Mach number profiles for Sod shock tube with constant $\gamma = 1.4$ (second-order accurate Van Leer scheme, limiters acting on the characteristic variables).

5.2.2 The Sod shock tube with variable γ

We have done similar comparisons of the different second-order accurate schemes for the Sod shock tube with variable γ (we again take $\gamma_L = 1.4$, $\gamma_R = 1.2$). We simply present on Figures 33 to 38 the results obtained with the second-order accurate Roe schemes of type (B) and (C).

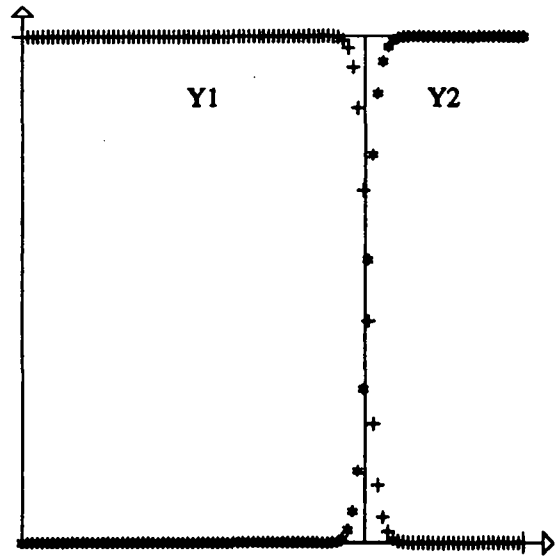

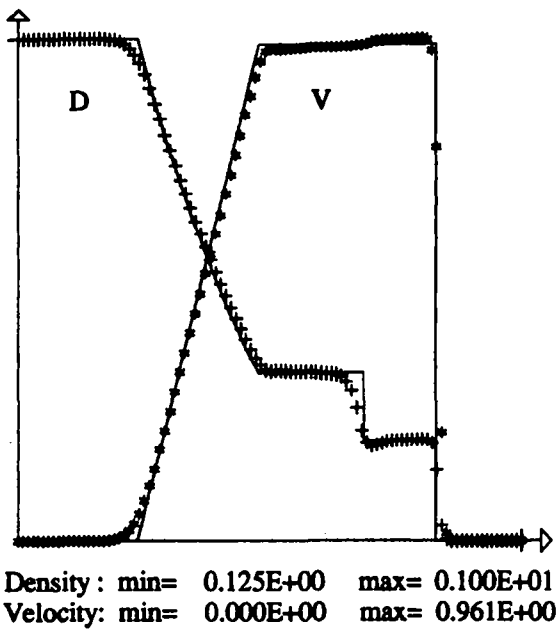

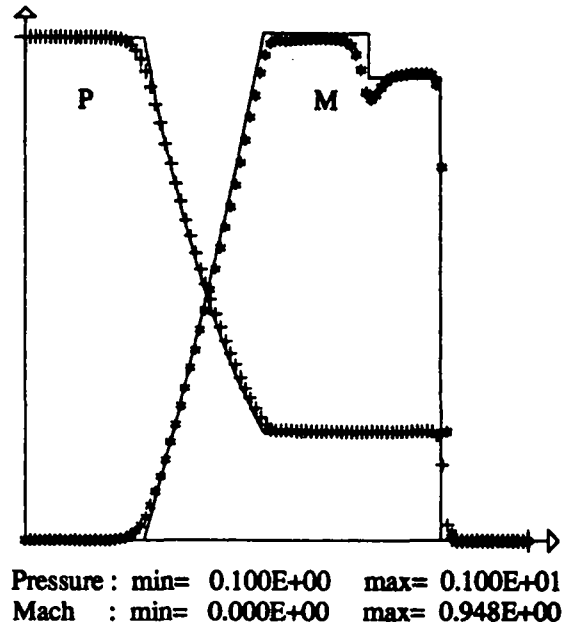

Figure 33: Mass fraction, density, velocity, pressure and Mach number profiles for Sod shock tube with variable γ (second-order accurate Roe scheme (B), limiters acting on the conservative variables).

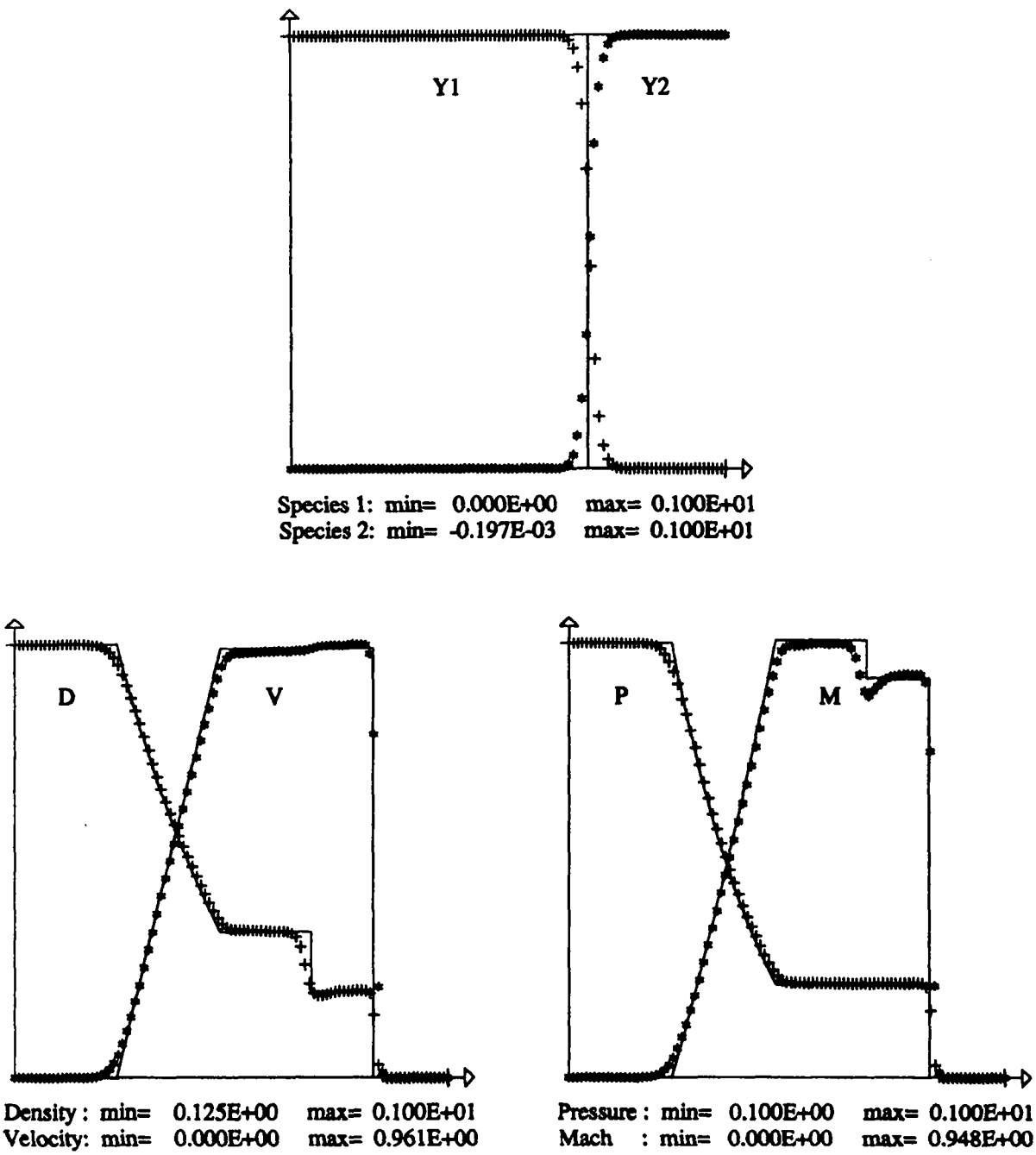

Figure 34: Mass fraction, density, velocity, pressure and Mach number profiles for Sod shock tube with variable γ (second-order accurate Roe scheme (B), limiters acting on the physical variables).

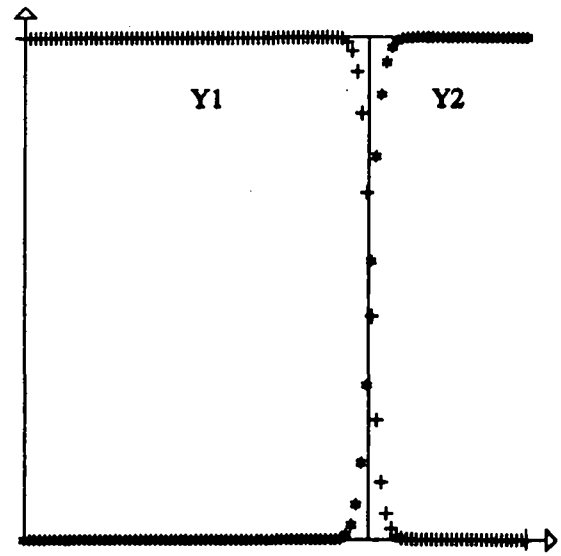

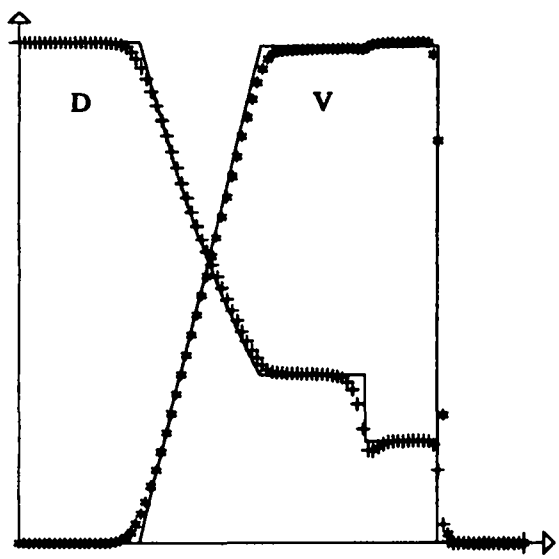

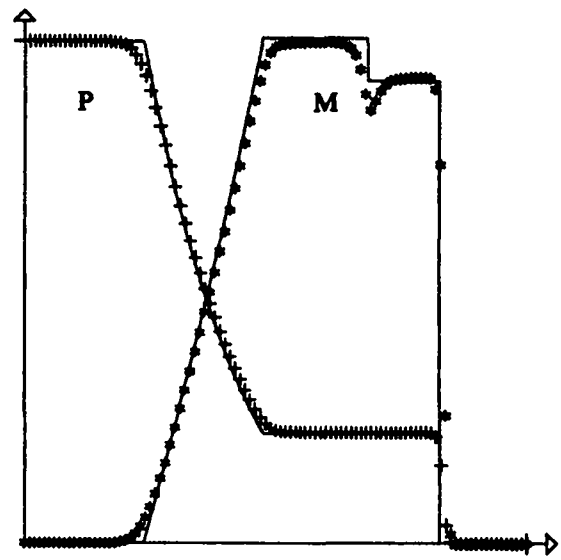

Figure 35: Mass fraction, density, velocity, pressure and Mach number profiles for Sod shock tube with variable γ (second-order accurate Roe scheme (B), limiters acting on the characteristic variables).

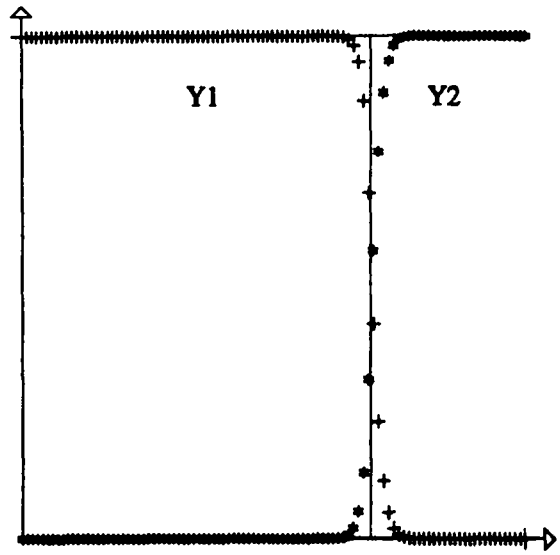

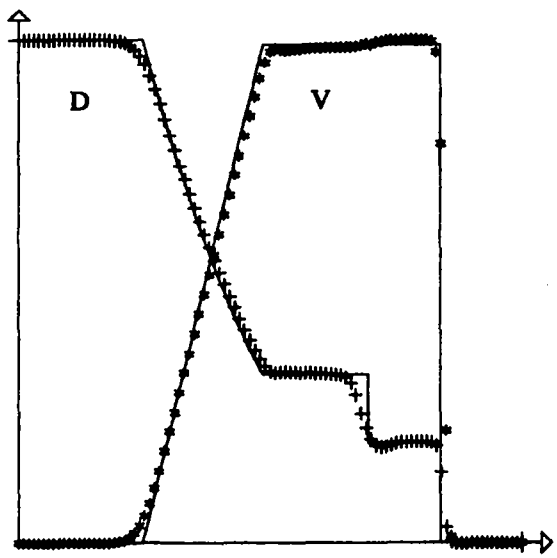

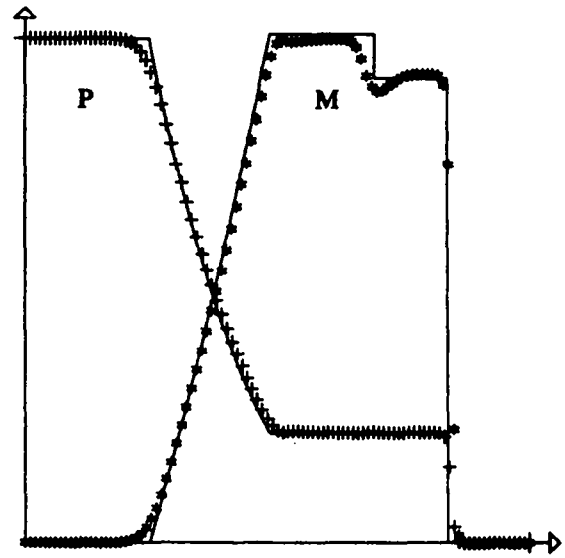

Figure 36: Mass fraction, density, velocity, pressure and Mach number profiles for Sod shock tube with variable γ (second-order accurate Roe scheme (C), limiters acting on the conservative variables).

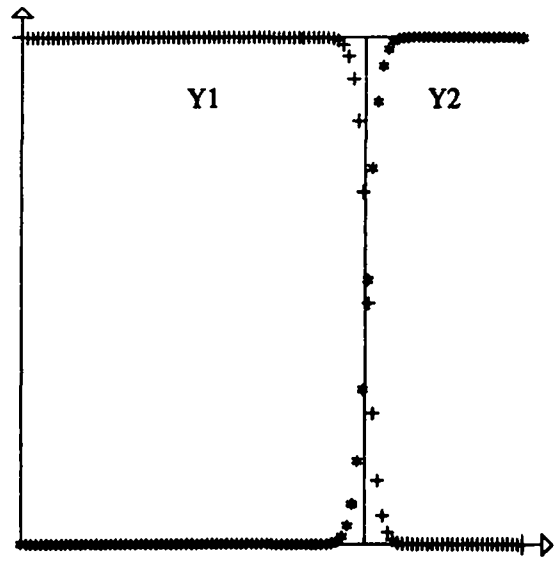

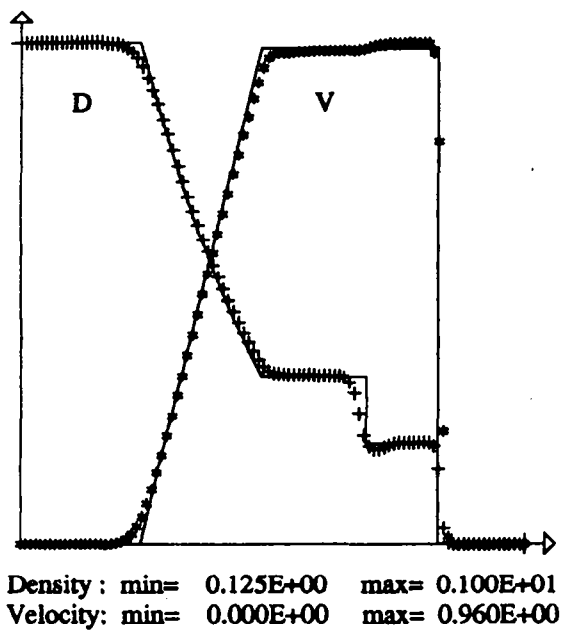

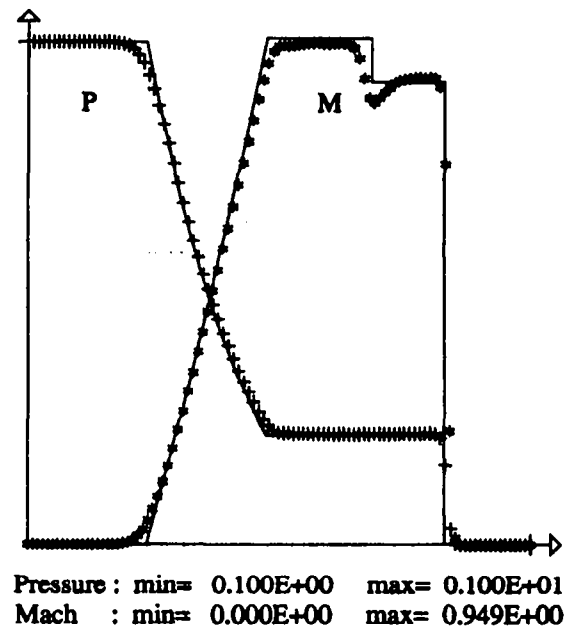

Figure 37: Mass fraction, density, velocity, pressure and Mach number profiles for Sod shock tube with variable γ (second-order accurate Roe scheme (C), limiters acting on the physical variables).

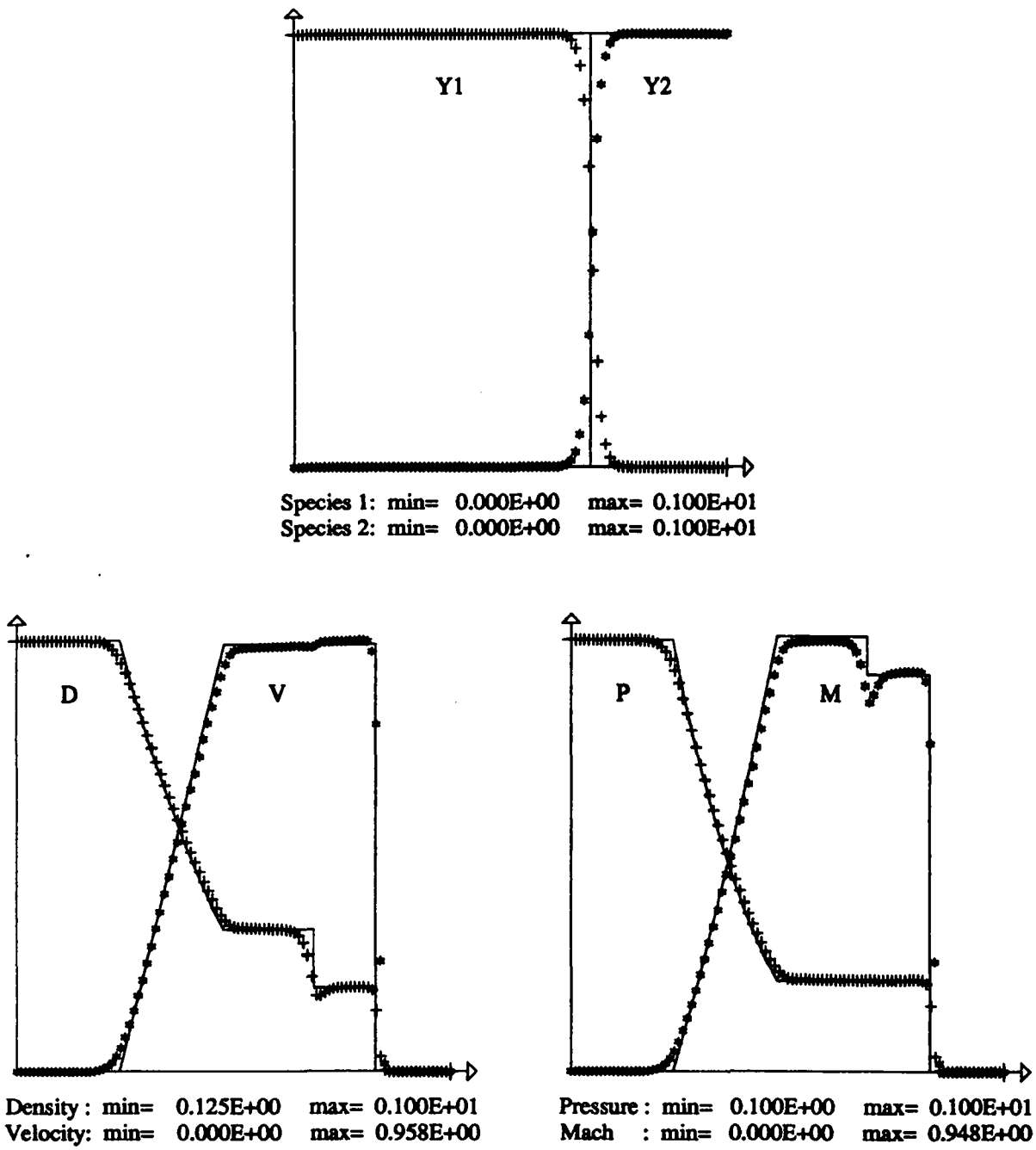

Figure 38: Mass fraction, density, velocity, pressure and Mach number profiles for Sod shock tube with variable γ (second-order accurate Roe scheme (C), limiters acting on the characteristic variables).

It is interesting to compare these results with those of Figures 24 to 32. Since γ is constant on each side of the contact discontinuity, one could think that the features of the present numerical results which are intrinsically due to the presence of two species can only be found in the neighbourhood of the contact discontinuity; in particular, one could think that the computed rarefaction wave, where γ has the value 1.4, should be exactly the same as in Figures 24 to 32. But such is not the case: the solution is now more diffused at the tail of the rarefaction wave, except in the case where limiters act on the conservative variables with approach (B) (see Figure 33, where the overshoot in the velocity profile has been aggravated, but where the solution is less diffused at the front of the rarefaction wave). We have to conclude that this excess of numerical diffusion is due to the fact that γ is not constant, and that it appears at the very beginning of the calculation, before the rarefaction wave and the contact discontinuity are well separated. At the contact discontinuity itself, we see that the slight discontinuity of the velocity again appears, and that an undershoot can be observed for the density on the right side of the contact discontinuity (this is particularly clear when the limiters act on the characteristic variables; see Figures 35 and 38). We again refer to Appendix B for a discussion of the effects of the variations of γ on the numerical results.

For the mass fractions, we again observe that minimal values of Y of the order of -10^{-3} are obtained with approach (B), whereas the approach (C) preserves the maximum principle when the limiters act on the physical variables. An unexpected observation is also that the width of the numerically smeared contact discontinuity measured on the mass fraction profiles is substantially reduced in Figure 33 (approach (B) with limiters acting on the conservative variables).

An important conclusion remains that the results of schemes (B) and (C) are again completely comparable, and that approach (C) remains a little cheaper than approach (B).

All the above conclusions also hold when the stiffer shock tube (64) is used to compare the different schemes.

6 CONCLUSIONS

In this study, we have considered three approaches for the computation of mixture flows: an uncoupled approximation (A) where the Euler equations for the mixture are solved with a classical upwind scheme using "frozen γ" and where the mass fraction equations are approximated by a donor cell scheme; a fully-coupled approximation (B) which uses a generalisation of the classical schemes designed for single-component inviscid flows to the complete system of the multi-component Euler equations, and a modified coupled approach (C) which relies on approach (B) but where the mass fraction equations are solved using the very upwinding of the continuity equations.

The main conclusions of the extensive comparisons presented above are the following. Clearly, the schemes which partially decouple the Euler equations and the species equations

using a "frozen γ approach" give unacceptable results. When γ is constant, all approaches give the same results for the hydrodynamical variables, whereas the results given by all approaches when γ actually varies are not quite as good as for constant γ. Moreover, these comparisons also show that modifying the multi-component Roe and Osher approximate Riemann solvers (B) as proposed in approach (C) enhances the quality of the computed results for the mass fraction: the schemes (C) actually preserve the maximum principle for the mass fraction, as predicted in Proposition 5 and Remark 6, without altering the results obtained for the hydrodynamical variables.

This advantage of schemes (C) over the unmodified Roe and Osher multi-component schemes (B) may reveal useful in many applications, including reactive flows. In particular, the fact that we have obtained here computed values of the mass fraction Y which are out of the interval $[0, 1]$ only by a small amount (10^{-3}) when using schemes (B) should not hide that the ability of these schemes to produce unphysical values of the mass fractions may well become much more unacceptable in other cases.

More generally, we have observed that the considered extensions of the Roe, Osher and Van Leer schemes to mixture flows roughly behave as the classical single-component Roe, Osher and Van Leer schemes for a shock tube problem, except at the contact discontinuity where additional difficulties appear if the specific heat ratio γ actually varies.

The last conclusion of the above calculations is that applying the slope limiters to the "physical variables" appears to be the best strategy for multi-component flows; this is undoubtedly true when schemes (C) are used, as suggested by Remark 6.

7 APPENDICIES

7.1 Appendix A

In this Appendix, we show that the multi-component Roe and Osher schemes (B) do not always preserve the maximum principle for the mass fraction.

Let us begin with the "physical Osher" scheme. The states W_L and W_R being considered given, we need to introduce some notations in order to detail equation (53). The path Γ connecting W_L and W_R is made of three pieces (we denote $\Gamma = \Gamma_1 \cup \Gamma_2 \cup \Gamma_4$), which are defined by the following properties: $\frac{dW}{ds}$ is parallel to the first eigenvector $r_1(W(s))$ on Γ_1, $\frac{dW}{ds}$ is parallel to the fourth eigenvector $r_4(W(s))$ on Γ_4, and $\frac{dW}{ds}$ lies in the eigenspace associated with the eigenvalue u on Γ_2. Furthermore, we call $W_{1/3}$ and $W_{2/3}$ the end points of Γ_2. Moreover, since the first characteristic field is genuinely non linear (see [3], [17]), there exists at most one point where λ_1 vanishes on Γ_1; this point, called a sonic point, is denoted $W^s_{1/3}$. In the same way, there exists at most one point $W^s_{2/3}$ where λ_4 vanishes on Γ_4.

Lastly, u is constant along Γ_2 since this eigenvalue is associated with a linearly degenerate characteristic field: we denote $u \equiv u^*$ on Γ_2 (see Figure 39).

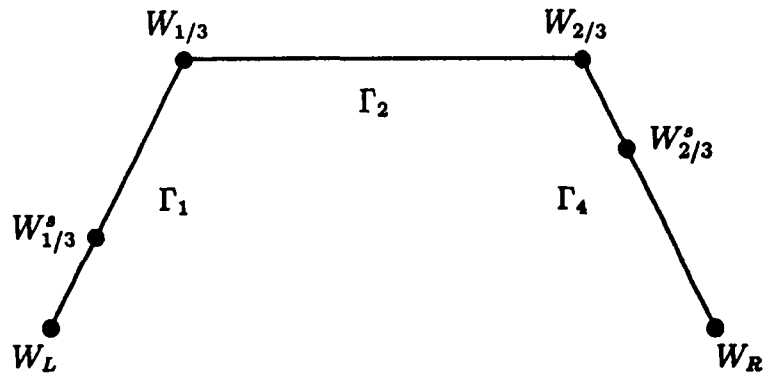

Figure 39: The path connecting W_L to W_R for the physical Osher scheme.

With these notations, the integral in (53) is easily evaluated. For instance, we have:

$$\begin{aligned} \int_{W_L}^{W^s_{1/3}} |A(W)|dW &= \int_{W_L}^{W^s_{1/3}} sign(\lambda_1(W))A(W)dW \\ &= sign(\lambda_1(W_L))[F(W^s_{1/3}) - F(W_L)] \,, \end{aligned} \tag{68}$$

since $sign(\lambda_1(W))$ is constant on the considered piece of Γ_1. Then, (53) can be rewritten as:

$$\begin{aligned} \Phi(W_L, W_R) &= \frac{F(W_L) + F(W_R)}{2} - \frac{sign(u^*)}{2}[F(W_{2/3}) - F(W_{1/3})] \\ &\quad -\frac{1}{2}\int_{\Gamma_1} |A(W)|dW - \frac{1}{2}\int_{\Gamma_4} |A(W)|dW \,. \end{aligned} \tag{69}$$

Since we know that the mass fraction Y is constant along Γ_1 and Γ_3, we can write the first and fourth components of the numerical flux under the form:

$$\Phi^1(W_L, W_R) = \Phi^1_+(W_L, W_R) + \Phi^1_-(W_L, W_R) \,, \tag{70}$$

$$\Phi^4(W_L, W_R) = Y_L\, \Phi^1_+(W_L, W_R) + Y_R\, \Phi^1_-(W_L, W_R) \,, \tag{71}$$

where:

$$\Phi^1_+(W_L, W_R) = \frac{F^1(W_L)}{2} - \frac{1}{2}\left(\int_{\Gamma_1} |A(W)|dW\right)^1 + \frac{sign(u^*)}{2}F^1(W_{1/3}) \,, \tag{72}$$

$$\Phi^1_-(W_L, W_R) = \frac{F^1(W_R)}{2} - \frac{1}{2}\left(\int_{\Gamma_4} |A(W)|dW\right)^1 - \frac{sign(u^*)}{2} F^1(W_{2/3}) \,. \tag{73}$$

Therefore, from (70) and (71), the "physical Osher" scheme (B) uses the same discrete mass fluxes for the continuity equation and for the species equation, as the schemes (C). But it is proved in [15] that, when (70)-(71) hold, a necessary and sufficient condition to preserve the maximum principle for the mass fraction is:

$$\Phi^1_+(W_L, W_R) \geq 0 \,, \quad \Phi^1_-(W_L, W_R) \leq 0 \,. \tag{74}$$

We can notive here that, for the multi-component Van Leer scheme, we have the relations:

$$\Phi^1(W_L, W_R) = F^1_+(W_L) + F^1_-(W_R) \,, \tag{75}$$

$$\Phi^4(W_L, W_R) = Y_L \, F^1_+(W_L) + Y_R \, F^1_-(W_R) \,, \tag{76}$$

which are very similar to (70)-(71). Moreover, it is easy to check that $F^1_+(W) \geq 0$ and $F^1_-(W) \leq 0$ for all W: in view of (74), this is the reason why the multi-component Van Leer scheme preserves the maximum principle for the mass fraction.

Unfortunately, (74) does not always hold for the "physical Osher" scheme. Tables A.1 and A.2 below, where we distinguish between 16 different cases, following Spekreijse [24], show when (74) holds or not:

	$u_L < c_L, u_R > -a_R$	$u_L > c_L, u_R > -a_R$
$c_{1/3} < u^*$	Yes(1)	Yes(5)
$0 < u^* < c_{1/3}$	Yes(2)	No (6)
$-c_{2/3} < u^* < 0$	Yes(3)	No (7)
$u^* < -c_{2/3}$	Yes(4)	No (8)

Table A.1: Maximum principle for the mass fraction using the "physical Osher" scheme.

	$u_L < c_L, u_R < -a_R$	$u_L > c_L, u_R < -a_R$
$c_{1/3} < u^*$	Yes(9)	Yes(13)
$0 < u^* < c_{1/3}$	Yes(10)	No (14)
$-c_{2/3} < u^* < 0$	Yes(11)	No (15)
$u^* < -c_{2/3}$	Yes(12)	No (16)

Table A.2: Maximum principle for the mass fraction using the "physical Osher" scheme.

We leave the details of the investigation to the reader.

We can illustrate these results by considering the shock tube problem defined by the relations:

$$\begin{cases} \rho_L = 1\,, & \rho_R = (1.4)^5\,, \\ u_L = 2\,, & u_R = 0\,, \\ p_L = (1.4)^{-1}\,, & p_R = (1.4)^6\,, \\ Y_L = 1\,, & Y_R = 0\,, \\ \gamma_L = 1.4\,, & \gamma_R = 1.4\,. \end{cases} \tag{77}$$

This problem corresponds to cases (6) and (7), which are the most likely to occur among all cases where (74) does not hold (see Spekreijse [24]). We chose it such that $W_{1/3} = W_{2/3} = W_R$.

Let i be such that $W_j^0 = W_L$ for all $j < i$ and $W_j^0 = W_R$ for all $j \geq i$. A straightforward calculation shows that, after one time step:

$$(\rho Y)_i^1 = \frac{\Delta t}{\Delta x}[(\rho u)_L - (\rho u)^*_{1/3}]\,, \tag{78}$$

$$(\rho)_i^1 = \rho_R + \frac{\Delta t}{\Delta x}[(\rho u)_L - (\rho u)^*_{1/3}]\,. \tag{79}$$

Since $[(\rho u)_L - (\rho u)^*_{1/3}] \approx -0.52$, we have $Y_{j_0}^1 < 0$, and the maximum principle is not preserved. Similarly, the same conclusions hold for the Osher-Solomon scheme.

Let us now consider the multi-component Roe scheme. It is easy to see that (70)-(71) also hold for the multi-component Roe scheme (B) (that is, that the multi-component Roe scheme also uses the same discrete mass fluxes for the continuity equation and the species equation). We have here:

$$\begin{aligned} \Phi_+^1(W_L, W_R) \;&= \rho_L(u_L + |\tilde{u}|) - |\tilde{u}|\frac{\sqrt{\rho_L}}{2(\sqrt{\rho_L}+\sqrt{\rho_R})}\frac{\Delta p}{\tilde{c}^2} \\ &+ \frac{\sqrt{\rho_L}}{\sqrt{\rho_L}+\sqrt{\rho_R}}\left(|\tilde{u}-\tilde{c}|\{\frac{\Delta p}{\tilde{c}^2} - \frac{\bar{\rho}\Delta u}{\tilde{c}}\} + |\tilde{u}+\tilde{c}|\{\frac{\Delta p}{\tilde{c}^2} + \frac{\bar{\rho}\Delta u}{\tilde{c}}\}\right), \end{aligned} \tag{80}$$

$$\begin{aligned} \Phi_-^1(W_L, W_R) \;&= \rho_R(u_R - |\tilde{u}|) + |\tilde{u}|\frac{\sqrt{\rho_R}}{\sqrt{\rho_L}+\sqrt{\rho_R}}\frac{\Delta p}{\tilde{c}^2} \\ &- \frac{\sqrt{\rho_R}}{2(\sqrt{\rho_L}+\sqrt{\rho_R})}\left(|\tilde{u}-\tilde{c}|\{\frac{\Delta p}{\tilde{c}^2} - \frac{\bar{\rho}\Delta u}{\tilde{c}}\} + |\tilde{u}+\tilde{c}|\{\frac{\Delta p}{\tilde{c}^2} + \frac{\bar{\rho}\Delta u}{\tilde{c}}\}\right), \end{aligned} \tag{81}$$

where $\bar{\rho} = \sqrt{\rho_L \rho_R}$, $\Delta u = u_L - u_R$, $\Delta p = p_L - p_R$.

To show that the multi-component Roe scheme (B) does not always preserve the maximum principle for the mass fraction, we simply exhibit now an example where (74) does not hold. We consider the shock tube problem defined by the relations:

$$\begin{cases} \rho_L = 1\,, & \rho_R = 1\,, \\ u_L = -1\,, & u_R = 1\,, \\ H_L = 1\,, & H_R = 5\,, \\ Y_L = 1\,, & Y_R = 0\,, \\ \gamma_L = 1.4\,, & \gamma_R = 1.4\,. \end{cases} \tag{82}$$

These values have been chosen so that all eigenvalues of the matrix $\tilde{A}$ are positive, which simplifies the expression of the fluxes since (45)-(46) then imply that $\Phi(W_L, W_R) = F(W_L)$. We have here $\Phi^1_+(W_L, W_R) = -1$, $\Phi^1_-(W_L, W_R) = 0$, and (74) does not hold.

7.2 Appendix B

In this Appendix, we discuss about the specific problems which appear when γ is not constant, and show that all upwind schemes considered above have difficulties in treating these problems.

As said before, the slight oscillations which appear at the contact discontinuity in the preceding multi-component results when γ is not constant are intrinsically related to the presence of several species. Following the analyses in [1] and [17], we analyse the origin of this difficulty by considering a Riemann problem (26) where the two states W_L and W_R are supersonic and can be separated by a contact discontinuity (more precisely, we assume that $u_L = u_R = \bar{u}$, $u_L > c_L$, $u_R > c_R$, $p_L = p_R = \bar{p}$). We further assume that we use an upwind scheme which satisfies:

$$\Phi(W_L, W_R) = F(W_L)\,, \tag{83}$$

in the present case, a natural condition since the states W_L and W_R are supersonic. After spatial discretization, we have at time $t = 0$: $W_j^0 = W_L$ for $j \leq i-1$, $W_j^0 = W_R$ for $j \geq i$. Using the consistency relation $\Phi(W, W) = F(W)$, it is easy to see that the values W_j^1 (updated values after one time step) are equal to W_j^0 for all $j \neq i$, and that W_i^1 is given by:

$$W_i^1 = W_R - \frac{\Delta t}{\Delta x}[F(W_R) - F(W_L)]\,. \tag{84}$$

Calling $\nu = \dfrac{\bar{u}\Delta t}{\Delta x}$ the Courant number ($0 \leq \nu \leq 1$ from the CFL stability condition), we easily deduce from (84) that:

$$\rho_i^1 = (1-\nu)\rho_R + \nu\rho_L\,, \tag{85}$$

$$Y_i^1 = \frac{(1-\nu)\rho_R Y_R + \nu\rho_L Y_L}{(1-\nu)\rho_R + \nu\rho_L}\,, \tag{86}$$

and:

$$u_i^1 = \bar{u} \,, \tag{87}$$

$$\frac{p_i^1}{\gamma(Y_i^1) - 1} = \bar{p} \left(\frac{1-\nu}{\gamma(Y_R) - 1} + \frac{\nu}{\gamma(Y_L) - 1} \right) . \tag{88}$$

Thus, after one time step, the velocity has the correct value at each node, but the pressure is modified at node i (since in general $p_i^1 \neq \bar{p}$). This inability of the scheme to reproduce from one time level to another the constant pressure $\bar{p}$ may well cause after several time steps the observed oscillations, and is *directly related to the fact that γ is not constant*, i.e. that the fluid is a mixture of several species.

Before investigating relation (88) in more detail, we want to point out that the preceding observation holds as soon as the assumption (83) is satisfied; in particular it holds even if an exact Riemann solver is used at each mesh interface $x_{j+1/2}$, as in the Godunov method, or with the Van Leer scheme. Only Glimm's scheme [10], which does not use the average process involved in Godunov-type schemes, would provide the correct pressure $p_i^1 = \bar{p}$. Another way to overcome this difficulty is to move the mesh points which are located in the neighbourhood of the contact discontinuity with the speed $\bar{u}$, as in the moving mesh method of Harten and Hyman [14].

For the sake of simplicity, let us now assume that $Y_L = 1$, $Y_R = 0$. Then (88) yields:

$$\frac{p_i^1}{\bar{p}} = \frac{\nu(\gamma_L - 1)\rho_L C_{vL} + (1-\nu)(\gamma_R - 1)\rho_R C_{vR}}{\nu \rho_L C_{vL} + (1-\nu)\rho_R C_{vR}} \left(\frac{1-\nu}{\gamma_R - 1} + \frac{\nu}{\gamma_L - 1} \right) . \tag{89}$$

Keeping all other parameters fixed, we consider the right-hand side of (89) as a function of γ_L and γ_R, denoted $f(\gamma_L, \gamma_R)$. Denoting $\alpha = \dfrac{\nu \rho_L C_{vL}}{(1-\nu)\rho_R C_{vR}}$ and $\beta = \dfrac{\nu}{1-\nu}$, we can rewrite:

$$f(\gamma_L, \gamma_R) = \frac{[\alpha(\gamma_L - 1) + \gamma_R - 1]\,[\beta(\gamma_L - 1) + \gamma_R - 1]}{(\alpha+1)(\beta+1)(\gamma_L - 1)(\gamma_R - 1)} . \tag{90}$$

We will consider now two different examples. We show on Figure 40 the plot of the function $\gamma_R \mapsto f(\gamma_L, \gamma_R)$ in the case where $\alpha = 2$, $\beta = 1$, for three values of γ_L. Obviously, it appears that, for the same value of $|\gamma_L - \gamma_R|$, the situation after one time step will be worse in the case when $\gamma_R < \gamma_L$ than in the case when $\gamma_R > \gamma_L$: for instance, we have $f(1.6, 1.2) > f(1.2, 1.6) > 1$.

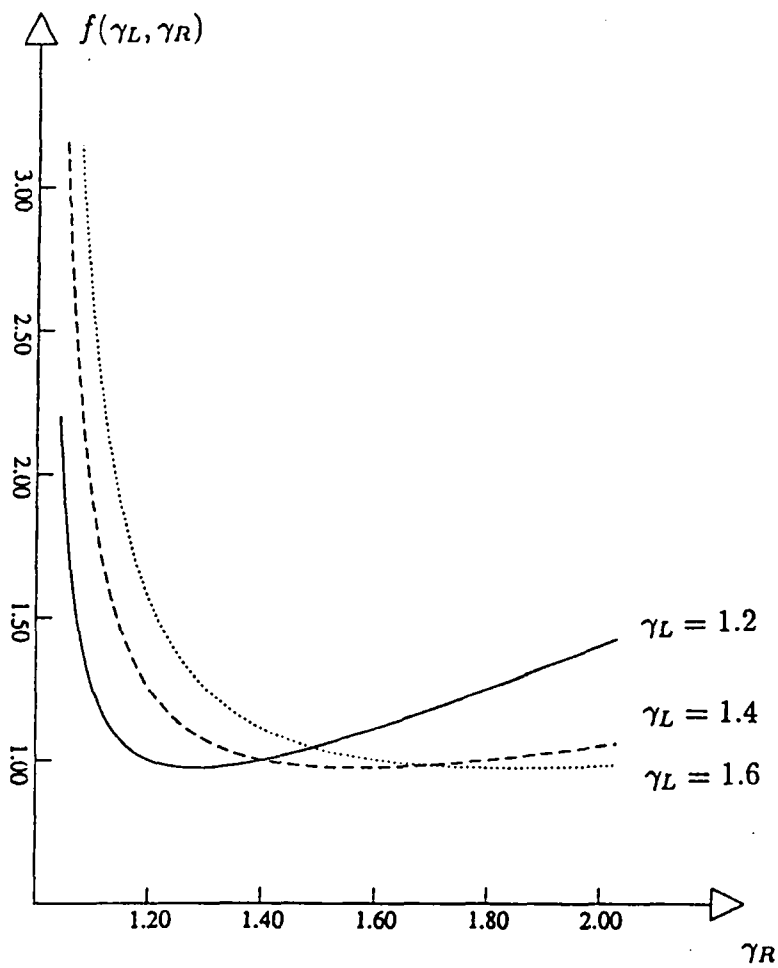

Figure 40: The plot of $f(\gamma_L, \gamma_R)$, for three values of γ_L ($\alpha = 2$, $\beta = 1$).

On the contrary, in the case where $\alpha = 0.5$ and $\beta = 1$, opposite conclusions arise, as shown by Figure 41; in particular, we have there $f(1.2, 1.6) > f(1.6, 1.2) > 1$.

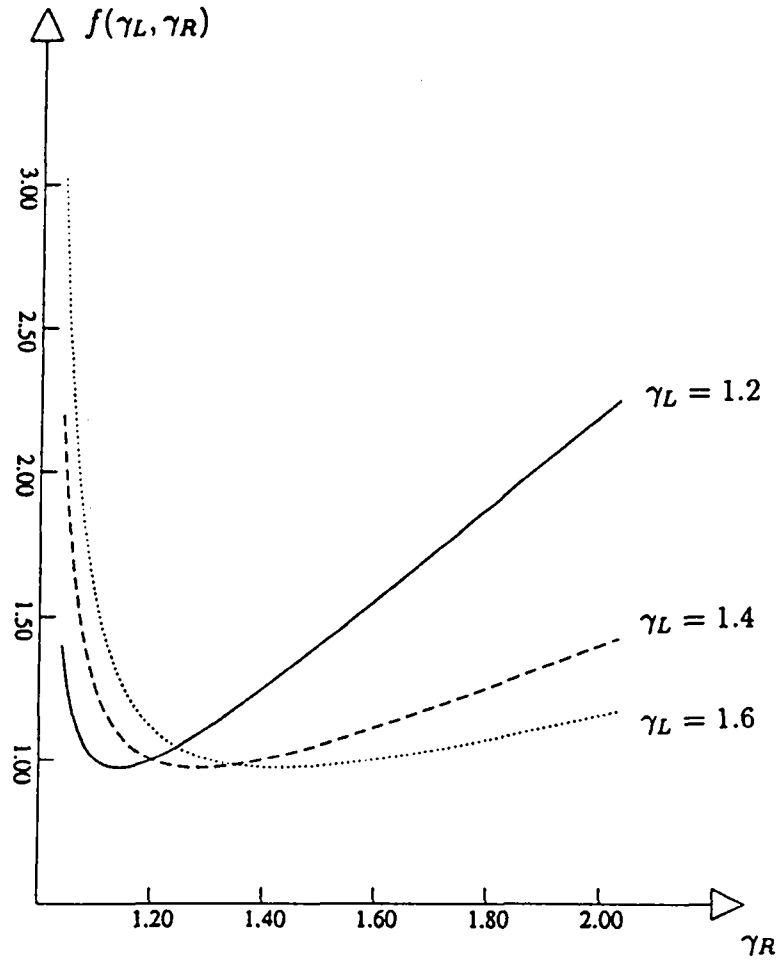

Figure 41: The plot of $f(\gamma_L, \gamma_R)$, for three values of γ_L ($\alpha = 0.5$, $\beta = 1$).

These conclusions can be illustrated by the following results. First, we consider the Sod shock tube (which corresponds to a situation where $\alpha > \beta$ as in Figure 40 since the density decreases across the contact discontinuity), with two different cases: for Figure 42, we take $\gamma_L = 1.2$, $\gamma_R = 1.6$, whereas we take $\gamma_L = 1.6$ and $\gamma_R = 1.2$ for Figure 43. Clearly, the results of Figure 43 are worse than those of Figure 42.

Similarly, we also consider the stiffer shock tube (which corresponds to a situation where $\alpha < \beta$ as in Figure 41 since the density increases across the contact discontinuity), with two different cases: $\gamma_L = 1.6$, $\gamma_R = 1.2$ (Figure 44), and $\gamma_L = 1.2$, $\gamma_R = 1.6$ (Figure 45). Here, the results of Figure 45 are worse.

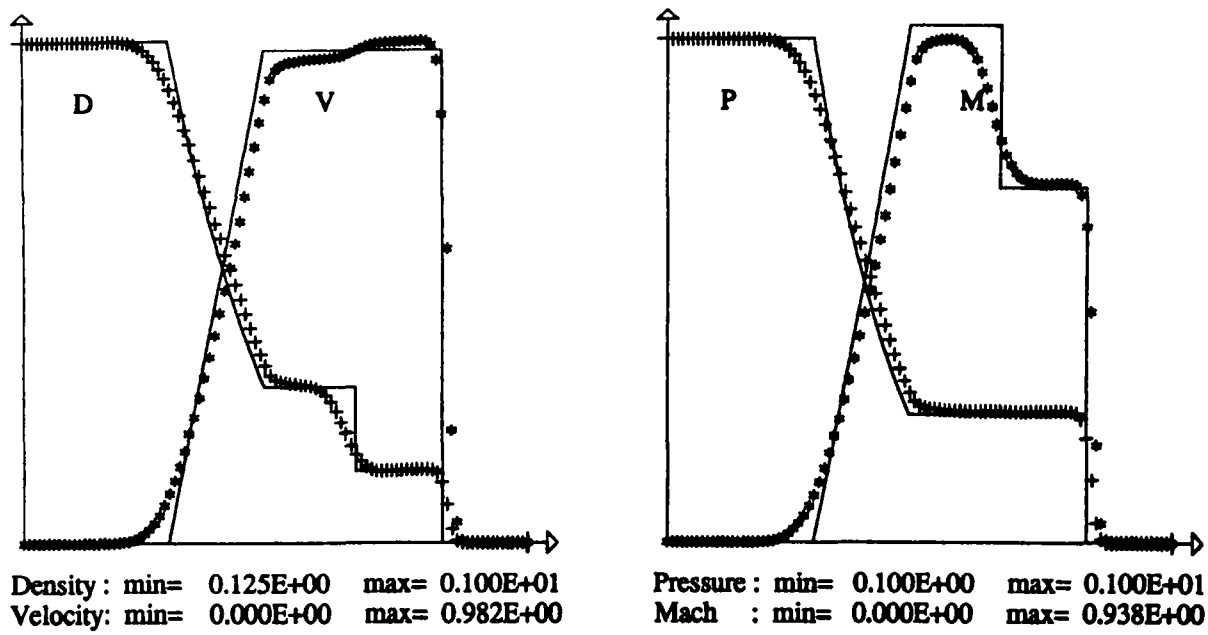

Figure 42: Density, velocity, pressure and Mach number profiles for Sod shock tube with $\gamma_L = 1.2$, $\gamma_R = 1.6$ (first-order accurate Roe scheme (C)).

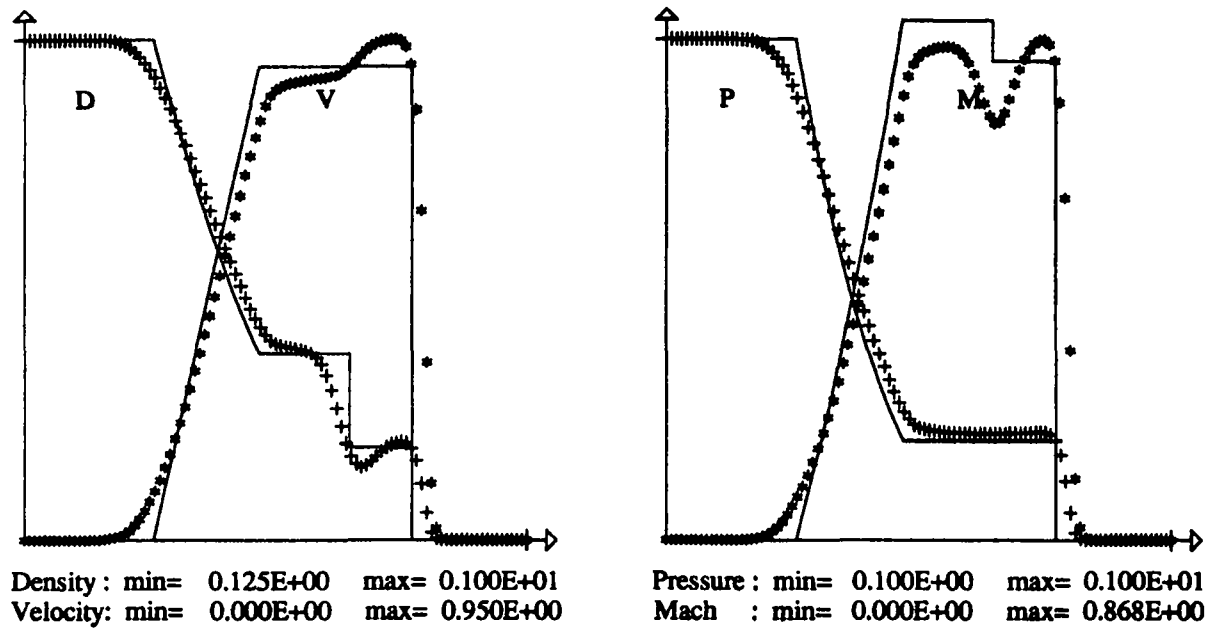

Figure 43: Density, velocity, pressure and Mach number profiles for Sod shock tube with $\gamma_L = 1.6$, $\gamma_R = 1.2$ (first-order accurate Roe scheme (C)).

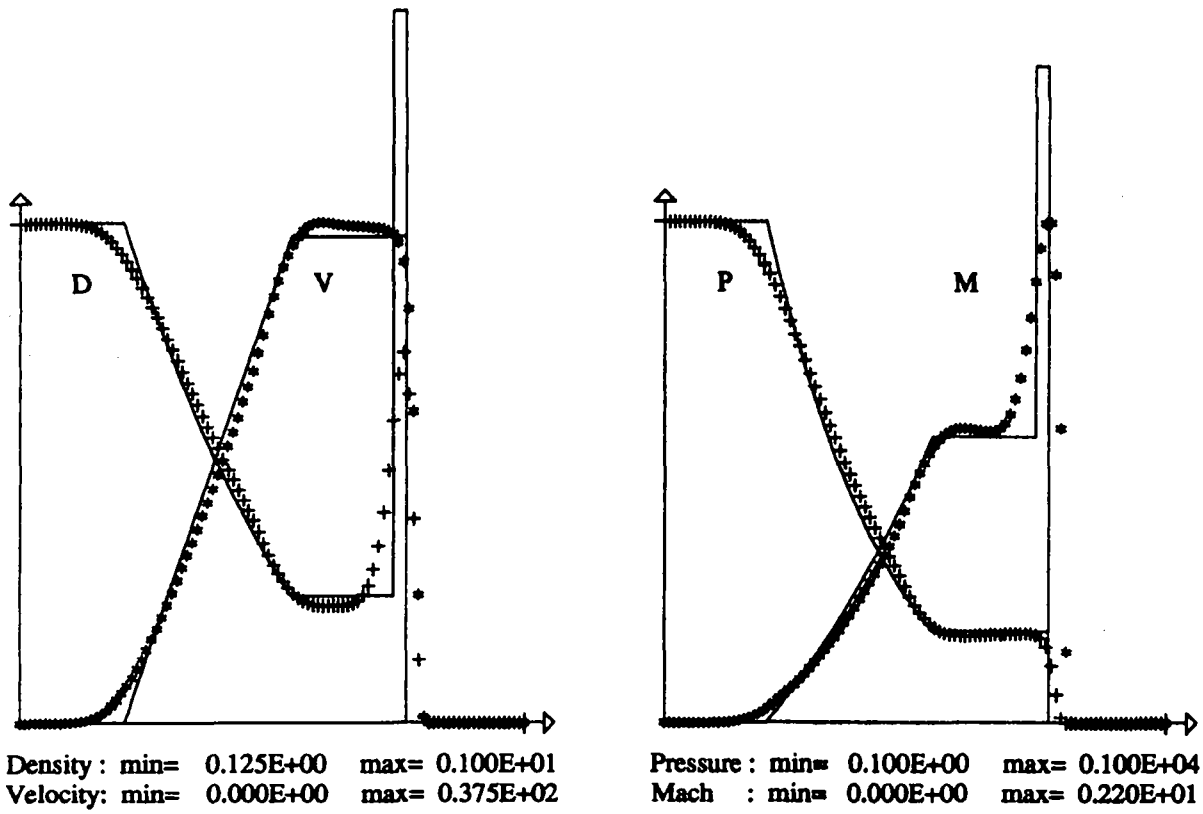

Figure 44: Density, velocity, pressure and Mach number profiles for the stiffer shock tube with $\gamma_L = 1.6$, $\gamma_R = 1.2$ (first-order accurate Roe scheme (C)).

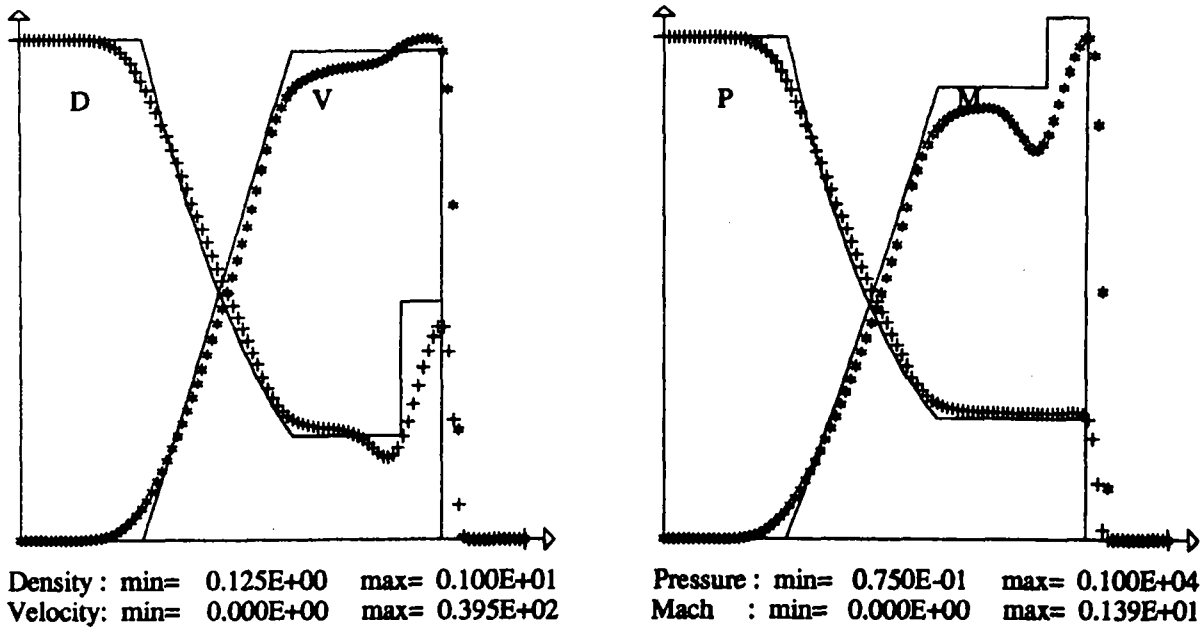

Figure 45: Density, velocity, pressure and Mach number profiles for the stiffer shock tube with $\gamma_L = 1.2$, $\gamma_R = 1.6$ (first-order accurate Roe scheme (C)).

Of course the previous analysis based on relations (89)-(90) only applies for the first time step, in a very special situation. Therefore, it just gives some insight on the reason why rather poor results are obtained in the neighbourhood of the contact discontinuity in Figures (42) to (45). The main conclusion of this Appendix is only qualitative: all upwind schemes considered in this paper do not behave well in the presence of strong variations of γ.

Remark B.1: Concerning the numerical solution of a contact discontinuity, we can add here another comment: it is easy to check that, in the single-component case, the schemes of Roe and Osher exactly solve a steady contact discontinuity, whereas the Van Leer scheme does not. We leave it to the reader to check that, in the multi-component case, the Roe and Osher schemes (B) and (C) still exactly solve a steady contact discontinuity, while the Van Leer scheme (B) still fails to solve it exactly. To remedy this, one could think of introducing a Van Leer scheme (C) constructed using relation (56); unfortunately, this Van Leer scheme (C) exactly solves a steady constact discontinuity only if γ and ρ are constant across this discontinuity, that is only if Y is the sole discontinuous variable. •

References

[1] R. ABGRALL, "Généralisation du schéma de Roe pour le calcul d'écoulements de mélanges de gaz à concentrations variables", La Recherche Aérospatiale, **6**, pp.31-43, (1988).

[2] R. ABGRALL, "Extension of Roe's approximate Riemann solver to equilibrium and non equilibrium flows", Proceedings of the eighth GAMM conference on numerical methods in fluid mechanics, Wesseling ed., Notes on Numerical Fluid Mechanics, **29**, pp. 1-10, Vieweg, Braunschweig, (1990).

[3] R. ABGRALL & J. L. MONTAGNE, "Généralisation du schéma d'Osher pour le calcul d'écoulements de mélanges de gaz à concentrations variables et de gaz réels", La Recherche Aérospatiale, **4**, pp. 1-13, (1989).

[4] G. V. CANDLER & R. W. McCORMACK, "The computation of hypersonic flows in chemical and thermal nonequilibrium", Paper N^o 107, Third National Aero-Space Plane Technology Symposium, (1987).

[5] D. CHARGY, A. DERVIEUX & B. LARROUTUROU, "Upwind adaptative finite-element investigations of the two-dimensionnal transonic reactive flows", Int. J. Num. Meth. Fluids, (1990), to appear.

[6] A. DERVIEUX, L. FEZOUI & B. LARROUTUROU, "Upwind numerical methods for compressible flows", to appear.

[7] J. A. DESIDERI, N. GLINSKY & E. HETTENA, "Hypersonic reactive flow computations", Computers and Fluids, **18**, (2), pp. 151-182, (1990).

[8] G. FERNANDEZ "Implicit conservative upwind schemes for strongly transnsient Flows", INRIA Report N^0 **873**, (1988).

[9] G. FERNANDEZ & B.LARROUTUROU, "Hyperbolic schemes for multi-component Euler equations", Nonlinear hyperbolic equations - Theory, numerical methods and applications, Ballmann & Jeltsch eds. pp. 128-138, Notes on numerical Fluid Mechanics, **24**, Vieweg, Braunschweig, (1989).

[10] J. GLIMM, "Solutions in the large for non linear hyperbolic systems of equations", Comm. Pure Appl. Math., **18**, pp. 697-715, (1965).

[11] N. GLINSKY, L. FEZOUI, M. C. CICCOLI & J. A. DESIDERI, "Non-equilibrium hypersonic flow computations by implicit second-order upwind finite elements", Proceedings of the eighth GAMM conference on numerical methods in fluid mechanics, Wesseling ed., Notes on Numerical Fluid Mechanics, **29**, pp. 159-168, Vieweg, Braunschweig, (1990).

[12] A. HABBAL, A. DERVIEUX, H. GUILLARD & B. LARROUTUROU, "Explicit calculations of reactive flows with an upwind finite-element hydrodynamical code", Rapport INRIA 690, (1987).

[13] A.HARTEN, P.D. LAX & B. VAN LEER "On upstream differencing and Godunov type schemes for hyperbolic conservation laws", SIAM Review, **25**, pp. 35-61, (1983).

[14] A. HARTEN & J. M. HYMAN, "A self-adjusting grid for the computation of weak solutions of hyperbolic conservation laws", J. Comp. Phys., **50**,(2), pp. 235-269, (1983).

[15] B. LARROUTUROU, "How to preserve the mass fraction positivity when computing compressible multi-component flows", J. Comp. Phys., to appear.

[16] B. LARROUTUROU, "Recent progress in reactive flow computations", Computing methods in applied sciences, Glowinski ed., SIAM, (1990), to appear.

[17] B. LARROUTUROU & L. FEZOUI, "On the equation of multi-component perfect or real gas inviscid flow", "Non linear hyperbolic problems", Carasso Charrier Hanouzet & Joly eds., Lecture Notes in Mathematics, **1402**, pp. 69-98, Springer Verlag, Heidelberg, (1989).

[18] A. MAJDA, "High Mach number combustion", Combustion and chemical reactors, Ludford ed., Lecture in Appl. Math., **24**, (1), pp. 109-184, AMS, Providence, (1986).

[19] J. L. MONTAGNE, H. C. YEE & M. VINOKUR, "Comparative study of high-resolution shock capturing schemes for a real gas", NASA Technical memorandum 100004, (1987).

[20] S. OSHER & F. SOLOMON, "Upwind difference schemes for hyperbolic systems of conservation laws, Journal Math. Comp., **38**, (158), pp. 339-374, (1982).

[21] P. L. ROE, "Approximate Riemann solvers, parameters vectors and difference schemes", J. Comp. Phys, **43**, p. 357, (1981).

[22] P. L. ROE, "Some contributions to the modelling of discontinuous flows", Proc. AMS/SIAM Seminar, San Diego, (1983).

[23] G.A. SOD' "A survey of several finite difference methods for systems of nonlinear hyperbolic conservation laws", J. Comp. Phys., **27**, pp. 1-31, (1977).

[24] S. P. SPEKREIJSE, "Multigrid solution of the steady Euler equations", Thesis, Delft University of Technology, (1987).

[25] P. K. SWEEBY, "High resolution schemes using flux limiters for hyperbolic conservation laws", SIAM J. Num. Anal., **21**, pp. 995-1011, (1984).

[26] B. VAN LEER, "Towards the ultimate conservative difference scheme II - Monotonicity and conservation combined in a second-order scheme", J. Comp. Phys., **14**, pp. 361-370, (1974).

[27] B. VAN LEER, "Flux-vector splitting for the Euler equations", Eighth international conference on numerical methods in fluid dynamics, Krause ed., pp. 507-512, Lecture notes in physics, **170**, Springer-Verlag, (1982).

[28] B. VAN LEER, J. L. THOMAS, P. L. ROE & R. W. NEWSOME, "A comparison of numerical flux formulas for the Euler and Navier-Stokes equations", AIAA paper 87-1104, (1987).

[29] F.A WILLIAMS, "Combustion théory", second edition, Benjamin Cummings, Menlo Park, (1985).

[30] H. C. YEE, "Upwind and symmetric shock capturing schemes", NASA Technical memorandum 89464, (1987).

Imprimé en France
par
l'Institut National de Recherche en Informatique et en Automatique

ISSN 0249 - 6399

ISSN 0249-6399